NOVEL ELECTROCATALYST SUPPORTS FOR POLYMER ELECTROLYTE FUEL CELLS

By

JONATHAN GOH

Thesis submitted in accordance with the requirements of

The University of Birmingham for the degree of

MASTER OF RESEARCH

School of Chemical Engineering

College of Engineering and Physical Sciences

The University of Birmingham

January 2014

ACKNOWLEDGMENTS

First and foremost I would like to thank my family for their constant support and encouragement throughout my extended stay away from home. You are truly irreplaceable and this work is dedicated to you. My heartfelt thanks also go to my aunt who helped to fund my studies, but more importantly for your unfailing faith in my abilities and potential.

It has also been a great honour and pleasure to have Prof Bruno G Pollet and Dr Surbhi S Sharma. You input has always been invaluable to me and I apologise if at times I did not perform up to your expectations. You always gave me the right kind of help, advice and direction that the circumstance dictated. (Thank you Surbhi, for allowing me to use your research material as part of my work when my project aims had to be shifted)

Special thanks to Dr Du Shangfeng, Dr Aman Dhir, Lynn Draper and John Hooper for always providing me with academic, technical and administrative support; sometimes even before I asked for it. You are now treasured friends.

Big thanks to my closest friends and colleagues – specifically Kevin, Gaurav, Geoff, Amrit, Mariska, James and Phil - and everyone else who supported me throughout my time as a part of the Hydrogen and Fuel Cell Research Group.

Thank you Dr Jill Newton, without your earlier work this would not be even remotely possible. Furthermore, both you and Amrit Chandan offered me the use of your samples for testing; the results of which have been included in this work.

Thank you Dr Oliver Curnick, even after you left the group you still remain a great source of help and guidance to anyone who asks.

To Dr Neil Rees, who must be the kindest person I have never met! Thank you for putting up with me and my delays; for your understanding and for your patience. You have taught me more than anyone else about scientific communication and I certainly would not have been able to produce this thesis without your help.

ABSTRACT

Pre-fabricated novel electrocatalysts for Polymer Electrolyte Fuel Cells (PEFCs) – Platinum supported on partially reduced graphene oxide (Pt/GO) and Platinum nanoparticles prepared with surfactant NP-9 supported on carbon (Pt/C NP-9) – were electrochemically characterised *ex situ* and evaluated against commercial Pt/C electrocatalysts obtained from Tanaka Kikinzokou TEC 10E50E (TKK Pt/C). It was observed that the TKK Pt/C outperformed the novel electrocatalysts in terms of ECSA (TKK = 84.69 m^2/g; Pt/C NP-9 = 8.39 m^2/g; Pt/GO = 22.10 m^2/g), besides demonstrating much better stability and consistency. However, the Pt/C NP-9 showed the best durability after accelerated degradation testing up to 20400 cycles. This result was attributed to the shielding effect of surfactant molecules on the surface of Pt clusters. The Pt/C NP-9 catalyst also showed the highest specific activity at 0.9 V (807.67 $\mu A/cm^2$) and 0.95 V (168.37 $\mu A/cm^2$), while the Pt/GO had the lowest specific activity and mass activity values. It is hypothesised that the Pt/GO catalyst performed poorly due to its structural characteristics i.e. graphene nanosheets obstruct mass transport of reactant gases to the Pt active sites.

Contents

1.0 Introduction 1

  1.1 Background – Fossil Fuels and Climate Change 1

  1.2 The Search for New Energy Sources 4

    1.2.1 Nuclear Energy 4

    1.2.2 Renewable Energy 5

  1.3 Hydrogen for the Future 6

    1.3.1 The Hydrogen Economy 6

    1.3.2 Fuel Cells & Hydrogen 7

    1.3.3 Polymer Electrolyte Fuel Cells (PEFC) 10

2.0 Literature Review 13

3.0 Aims & Objectives 18

4.0 Experimental 19

  4.1 Scope of work 19

  4.2 Experiment setup 20

    4.2.1 Counter electrode 21

    4.2.2 Reference Hydrogen Electrode 22

    4.2.3 Working Electrode 24

    4.2.4 Electrochemical Cell & Glassware cleaning 26

  4.3 Preparation of Catalyst Ink 28

    4.3.1 Pt/C with NP9 surfactant 28

    4.3.2 Pt/GO 30

    4.3.3 Pt/C from commercial TEC 10E50E Pt catalyst 31

  4.4 Experimental Procedures 31

    4.4.1 Autolab GPES Procedures for CV and ORR tests 31

5.0 Results & Discussion 37
  5.1 Cyclic Voltammetry and ECSA 37
  5.2 ORR Catalyst Activity 42
  5.3 Catalyst Degradation 45
  5.3 Correlation between Structure and Performance 49
  5.4 Other Observations 52
6.0 Conclusions & Recommendations 54
  6.1 Conclusions 54
  6.2 Recommendations 55
7.0 References 57
8.0 Appendices 64
  8.1 Appendix 1 – Data Tables 64
    8.1.1 TKK Pt/C 64
    8.1.2 Pt/C NP-9 65
    8.1.3 Pt/GO 66
    8.1.4 Catalyst Activity 67
  8.2 Appendix 2 – Graphs 68
    8.2.1 TKK Pt/C 68
    8.2.2 Pt/C NP-9 70
    8.2.3 Pt/GO 72
  8.3 Conferences Attended 74

Table of Tables

Table 1 Comparison of Fuel Cell Technologies (Source: US DOE EERE) 9
Table 2 Half wave potentials obtained from LSV at 1600 rpm 43
Table 3 Summary of ORR-evaluated specific area (SA) and mass (MA) activities 44
Table 4 ECSA values obtained from linear CV for TKK Pt/C (pre-ORR) 64
Table 5 ECSA values obtained from linear CV for TKK Pt/C (post-ORR) 64
Table 6 ECSA values after cycles of ADT for TKK Pt/C 65
Table 7 ECSA values obtained from linear CV for Pt/C NP-9 (pre-ORR) 65
Table 8 ECSA values obtained from linear CV for Pt/C NP-9 (post ORR) 66
Table 9 ECSA values after cycles of ADT for commercial Pt/C NP-9 66
Table 10 ECSA values obtained from linear CV for Pt/GO (pre-ORR) 66
Table 11 ECSA values obtained from linear CV for Pt/GO (post-ORR) 67
Table 12 ECSA values after cycles of ADT for commercial Pt/GO 67
Table 13 ORR-evaluated catalyst specific area (SA) and mass (MA) activities 67

Table of Figures

Figure 1 - Distribution of fossil fuel reserves around the world (Source: The Carbon Brief, 2013) 3
Figure 2 - The closed system of a battery (left) and the open system of a fuel cell (right) 8
Figure 3 - Schematic diagram of (a) typical PEFC and (b) single cell fuel cell (Source: US DOE Fuel Cell Handbook) 11
Figure 4 - Schematic illustration of the model of surfactant protected Pt clusters (a) Pt cluster embedded in the hydrophobic domain of the micelle, and (b) Pt cluster adsorbed by the alkyl parts of the molecules on its surface (Source: Yonezawa et al. [24]) 14
Figure 5 - Schematic of electrochemical cell setup 21
Figure 6 - Counter electrode affixed with a rubber stopper to maintain an airtight connection with the electrochemical cell 22
Figure 7 - Schematic of self-made Reference Hydrogen Electrode (RHE) 22
Figure 8 - Setu for blowing dry GCEs before ink application 25
Figure 9 - Characteristic regions of a cyclic voltammogram for Pt 33
Figure 10 - CVs at different scan rates for TKK Pt/C in deoxygenated 0.1 M $HClO_4$, 25 °C 37
Figure 11 - Average ECSA for commercial TKK Pt/C at various scan rates 38
Figure 12 - Average ECSA values for Pt/C NP-9 at various scan rates 39
Figure 13 - Average ECSA values for Pt/GO at various scan rates 40
Figure 14 - Overlaid CVs for TKK Pt/C, Pt/C NP-9 and Pt/GO (20 mV/s) 40
Figure 15 - Comparison of LSV scans (worst TKK/Pt/C against the best Pt/C NP-9 and Pt/GO) at 10 mV/s and 1600 rpm 42
Figure 16 - Average ECSA degradation for (A) TKK Pt/C, (B) Pt/C NP-9, and (C) Pt/GO 46
Figure 17 - Diagrammatic illustration of surfactant interactions with Pt nanoparticles 49
Figure 18 - Diagrammatic illustration of general GO orientation in the catalyst film 50
Figure 19 - Pre- vs Post-ORR ECSA values 52
Figure 20 - Linear CV for TKK Pt/C in 0.1 m $HClO_4$ 68
Figure 21 - LSV for TKK Pt/C in oxygen saturated 0.1 M $HClO_4$ 68
Figure 22 - Pre- vs Post-ORR Linear CV for TKK Pt/C in 0.1 M $HClO_4$ 69
Figure 23 - ADT ECSA profile for TKK Pt/C in 0.1 M $HClO_4$ 69
Figure 24 - Linear CV for Pt/C NP-9 in 0.1 M $HClO_4$ 70
Figure 25 - LSV for Pt/C NP-9 in oxygen saturated 0.1 M $HClO_4$ 70
Figure 26 - Pre- vs Post-ORR Linear CV for Pt/C NP-9 in 0.1 M $HClO_4$ 71
Figure 27 - ADT ECSA profile for Pt/C NP-9 in 0.1 M $HClO_4$ 71
Figure 28 - Linear CV for Pt/GO in 0.1 M $HClO_4$ 72
Figure 29 - LSV for Pt/GO in oxygen saturated 0.1 M $HClO_4$ 72
Figure 30 - Pre- vs Post-ORR Linear CV for Pt/GO in 0.1 M $HClO_4$ 73
Figure 31 - ADT ECSA profile for Pt/GO in 0.1 M $HClO_4$ 73

1.0 Introduction

1.1 Background – Fossil Fuels and Climate Change

The commercialisation of oil coupled with the invention of the steam engine undoubtedly catalysed the global industrial revolution of the 18th and 19th century. Starting in the mid-1700s, mankind's newfound ability to convert raw fuel into power on a consistent basis resulted in production lines with massive output capabilities and widely expanded distribution channels. This timely development was necessary to fulfil the ever increasing demands of a population in rapid growth.

The high energy density of oil and coal has made them invaluable resources even to this day. However, these and other fossils fuels exist in a finite amount within the Earth's crust. Fossils fuels were formed from decomposed prehistoric life subject to high pressures and temperatures deep underground over millions of years; this explains the limited supply available and also the complications in extracting some forms of fossil fuels. Upon successful extraction of fossil fuels, some processing is still required to minimise pollution and to obtain the useful products from the raw material.

In the 21st century, fossils fuels are used not only for fuel i.e. petrol, diesel, kerosene, coal, natural gas etc., but also as the starting material for a myriad of chemicals and products. These include plastics (eg. nylon), inorganic fertilisers, fabrics (e.g. polyester, polyurethane), medicine, cosmetics and many other products that have become ubiquitous in society. This has rather exacerbated the problem of depleting fossil fuels and has also raised the urgency to reduce mankind's dependence on fossil fuels for energy, being non-recyclable/recoverable when used for this purpose.

Although it has been recently reported that new fossil fuel deposits (shale gas, tar sands, methane hydrates) have now been found in various places around the world [1,2], these entail more complicated, energy intensive extraction methods that could even result in other environmental impacts [3]. As such, careful evaluation of cost and benefits must be carried out before any decision is made. Questions such as the ones below must be addressed truthfully and responsibly by governments and scientists alike:

- does the amount of the resource available and its market value justify the cost of extraction?
- if estimates of reserves vary so frequently and widely, how far can these numbers be trusted?
- is opting to extract these newly discovered resources a means to ease the transition from fossil fuels to more renewable energy sources? Or is it simply prolonging the inevitable?
- will the use of these resources exacerbate our climate condition?
- how will the extraction of these resources affect our environment?

Ultimately, regardless of how many more reserves of fossil fuels lie undiscovered within the planet, the inescapable fact is that fossil fuels are finite and will be depleted if used continuously. Figure 1 shows the carbon emissions and fossil fuel reserves by regions in the world [4]. The responsible decision would be to reduce mankind’s dependence on fossil fuels and gradually (but urgently) shift our relationship with energy in terms of resource management and usage behaviour.

Figure 1 - Distribution of fossil fuel reserves around the world (Source: The Carbon Brief, 2013)

In the last 30 years, there has been an increasing level of concern with regards to unrestrained fossil fuel consumption. Prior to this, the link between elevated levels of carbon dioxide in the atmosphere and increased global temperature had already been made in 1896 by Swedish scientist Svante Arrhenius [5]. However Arrhenius predicted a longer timescale for warming and thus deemed it a beneficial and necessary phenomenon to maintain the Earth’s habitable temperature. This theory was later refuted by scientists and climatologists when further studies showed that the presence of carbon dioxide in the atmosphere continued to affect the rise in temperature in a vicious cycle.

The Kyoto Protocol of 1997 was a major milestone in addressing the issue as it represented the first step of inter-governmental acknowledgement and action towards anthropomorphic climate change. Nations that ratified the Kyoto Protocol were bound to reduce their carbon emissions through a series of time-orientated goals to help stabilise global temperatures. However, it has proven to be a challenge to amend more than 200 years of practises and infrastructure that have brought today's level of progress.

The signs and effects of climate change have been appearing all over the planet and its effects cannot be taken lightly. Excessively severe natural disasters such as hurricanes and typhoons have been more frequently reported besides melting ice caps, retreating glaciers and uncharacteristic flooding in places all around the globe. The lesson is universal and clear: climate change has and will have an impact on all life on the planet.

1.2 The Search for New Energy Sources

With ever increasing global awareness of depleting fossil fuel reserves, much attention has been directed towards identifying new energy sources. To avoid the energy issues of today, the energy resource(s) of the future must be sustainable, environmentally friendly, secure, cost effective and capable of expansion to accommodate an expanding population.

1.2.1 Nuclear Energy

There has never been another energy resource as polarising as nuclear energy. Until recently, nuclear energy was widely acknowledged to be the answer to the world's energy problems. However, in light of the 2011 Fukushima-Daichii nuclear disaster[1], opinions have been swayed due to the extensive damage and lasting impact of such events. Almost immediately following the meltdown, Germany cancelled its nuclear programme [6].

---

[1] On 11 March 2011, a tsunami off the coast of Japan triggered a series of equipment failures, nuclear meltdowns and radioactive material leakage at the Fukushima I Nuclear Power Plant. Afterward and still today, authorities are struggling to contain the radioactive water previously used to cool the reactors. The disaster received widespread news coverage and was the largest nuclear disaster since the Chernobyl disaster of 1986.

While nuclear power is undeniably one of the few resources capable of fulfilling base-load energy demand, public opinion regarding nuclear energy has deteriorated to the point where it is generally considered only as a last resort or as a means to smoothen the transition to another energy source.

1.2.2 Renewable Energy

Renewable energy refers to energy sources that are natural, sustainable and could potentially be used indefinitely without adverse effects on the planet. Renewable energy is not a foreign concept as historical records indicate its use in ancient civilisations as a means of powering simple mechanisms. The Greek engineer Heron was also noted to have invented a wind-powered organ as early as 1 AD [7]. Other notable uses for renewable energy include water wheels to mill grain or pound cotton into fabrics. In today's world, hydroelectricity is an example of renewable energy as dams and turbines convert potential energy of stored water into kinetic energy and subsequently electricity. This method does not come without its drawbacks though, as dams are often sited on rivers and result in large areas of natural forests being flooded and submerged to accommodate the massive volume of water required for its efficient use.

Other examples of renewable energy are solar, wind, tidal, wave, geothermal and biomass. All have the potential for extensive implementation along with their corresponding cost and benefits, not to mention unique limitations. For example, geothermal energy is omnipresent in seismically active regions such as Iceland and the *Ring of Fire* but would not be a worthwhile investment in countries with low seismic activity. Similarly, solar energy can be harvested effectively on a large scale in arid landscapes such as sub-Saharan Africa or central Australia but would be a high cost and low benefit investment in the temperate climate of northern Europe. Also, the most wind energy can be collected off-shore but the challenges of maintenance and risks associated with installing and operating a wind farm in rough seas remain a very real limitation.

The universal challenges typically associated with renewable energy resources are intermittency, inefficiency, cost of infrastructure, operation and maintenance, and transportability. Intermittency is a real issue especially since energy demand over a period of time is not uniformed. It is therefore imperative that whatever energy source is chosen has the ability and flexibility to deal with peak energy demands.

1.3 Hydrogen for the Future

It is a well-established fact that hydrogen is the most abundant element in the universe. In fact, the Sun consists of 75% hydrogen by weight. On earth however, hydrogen exists primarily in complex compounds. The use of hydrogen as an energy vector is logical and advantageous: hydrogen has a high energy density and its combustion yields water without any carbon emissions.

1.3.1 The Hydrogen Economy

The Hydrogen Economy was proposed in 1970 as the energy system of the future. Hydrogen, as previously mentioned, has a much higher energy density (142 MJ/kg) as compared to fossil fuels (47 MJ/kg) [8]. The Hydrogen Economy includes a four pronged approach of hydrogen production, delivery, storage and usage. Unfortunately, the physical and chemical contrasts between hydrogen and the fuels of today necessitate a large measure of consideration and investment before the Hydrogen Economy can be realised.

1.3.2 Fuel Cells & Hydrogen

Fuel cells have been the focus of much research and development over the past few years due to their versatility and environmental benefits. Many applications have been considered for fuel cells, notably in Combined Heat and Power (CHP) or stationary power systems, for vehicular transport either as the prime mover or range extenders for battery electric vehicles (BEV) and most recently as portable energy sources for personal electronic devices. Patents filed by Samsung® and Apple® recently for fuel cell powered devices are indicative of the increasing potential applications for fuel cells. Developers such as Tekion® have also patented designs for mobile phones [9] powered by Direct Formic Acid Fuel Cells (DFAFC) and provide further justification of the importance of fuel cells in the future.

It is apt at this juncture to define fuel cells and discern the differences between fuel cells and batteries, for the purpose of clarity. Both fuel cells and batteries are silent, electrochemical devices that convert chemical energy into electrical potential. The term silent is used to imply the absence of any mechanical components or moving part, unlike an internal combustion engine that facilitates the conversion of chemical energy to heat to mechanical motion. As such, fuel cells and batteries may be considered to be almost maintenance free. Both are also modular, implying that they may be arranged in series or parallel to increase the output of voltage or current respectively.

The difference between fuel cells and batteries lie in the nature of the systems. A battery is a closed system: once it is installed in an electrical circuit, it discharges current continuously until it is depleted. Once this occurs, the battery may be recharged (if possible) or preferably recycled. The electrical potential within the battery is produced when its chemical contents migrate from one electrode to the other; the energy from the battery is thus ‘depleted’ when the chemical transfer stops. As such, the lifetime of the battery is limited by the amount of chemical fuel present within the battery. A fuel cell is an open system in the sense that it continues to operate so long as the fuels are supplied, giving it an advantage over batteries in various applications and also validating its role as a range extender for BEVs.

Figure 2 shows simple schematic diagrams of a battery and a fuel cell, illustrating the closed and open nature of both systems.

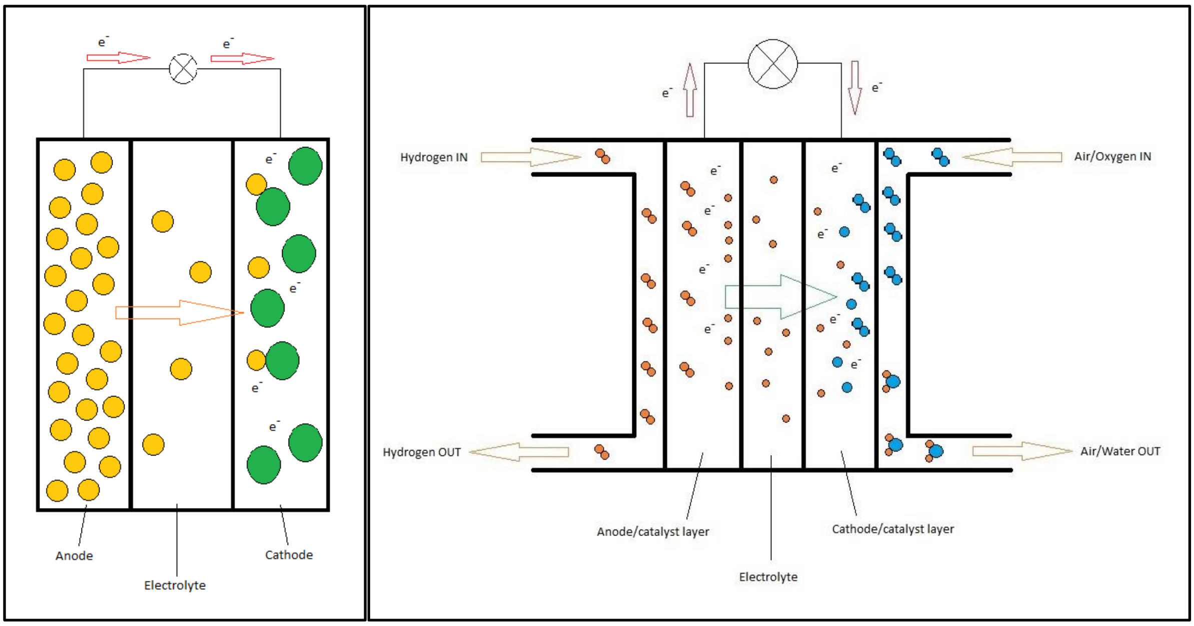

Figure 2 - The closed system of a battery (left) and the open system of a fuel cell (right)

There are several types of fuel cells being developed for commercial competitiveness and viability; the polymer electrolyte fuel cell (PEFC), direct methanol fuel cell (DMFC) and solid oxide fuel cell (SOFC) are three popular examples. Table 1 below summarises a few available fuel cell technologies, taken from the US Department of Energy's Energy Efficiency & Renewable Energy program website [10].

Fuel Cell Type	Common Electrolyte	Operating Temperature	Efficiency	Applications	Advantages	Disadvantages
Polymer Electrolyte (PEFC)	Perfluoro sulfonic acid	50-100°C (typically 80°C)	60% transportation, 30% stationary	• Backup power • Portable power • Distributed generation • Transportation • Specialty vehicles (forklifts, buses etc)	• Solid electrolyte reduces corrosion & electrolyte management problem • Low temperature • Quick start-up	• Expensive catalysts • Sensitive to fuel impurities • Low temperature waste heat
Alkaline (AFC)	Aqueous solution of potassium hydroxide soaked in a matrix	90-100°C	60%	• Military • Space	• Cathode reaction faster in alkaline electrolyte, leads to high performance • Low cost components	• Sensitive to CO_2 in fuel and air • Electrolyte management
Phosphoric Acid (PAFC)	Phosphoric acid soaking in a matrix	150-200°C	40%	• Distributed generation	• Higher temperature enables CHP • Increased tolerance to fuel impurities	• Platinum catalyst • Long start-up time • Low current and power
Molten Carbonate (MCFC)	Solution of lithium, sodium, and/or potassium carbonates soaked in a matrix	600-700°C	45-50%	• Electric utility • Distributed generation	• High efficiency • Fuel flexibility • Can use a variety of catalysts • Suitable for CHP	• High temperature corrosion and breakdown of cell components • Long start-up time • Low power density
Solid Oxide (SOFC)	Yttria stabilised zirconia	700-1000°C	60%	• Auxiliary power • Electric utility • Distributed generation	• High efficiency • Fuel flexibility • Can use a variety of catalyst • Solid electrolyte • Suitable for CHP • Hybrid/GT cycle	• High temperature corrosion and breakdown of cell components • High temperature operation requires long start-up time and limits

Table 1 Comparison of Fuel Cell Technologies (Source: US DOE EERE)

1.3.3 Polymer Electrolyte Fuel Cells (PEFC)

Of the examples listed in Table 1, the PEFC has been the most focused on. Using hydrogen as fuel, the PEFC has a big role to play in the Hydrogen Economy should it come to fruition. The PEFC offers several advantages, among which:

a) PEFCs produce minimal emissions; essentially combining protons from hydrogen with oxygen molecules to produce electricity, water and residual heat. Vehicular transport would particularly benefit from this, as exhaust emissions from combustion engines account for ca. 30% of all carbon emissions released into the atmosphere.

b) PEFCs have low operating conditions. This implies that energy can be drawn from fuel cells almost instantaneously when required, without excessive start-up times for warming up.

c) Hydrogen is the principal fuel for PEFCs. Although the most commercially viable source of hydrogen today is syngas from hydrocarbon streams, hydrogen is also most easily coupled with renewable energy sources.

The Hydrogen Oxidation Reaction (HOR) and the Oxygen Reduction Reaction (ORR) drive the PEFC, facilitated by platinum (Pt) catalysts on the electrodes. These reactions are given below:

HOR at anode: $H_2 \rightarrow 2H^+ + 2e^-$ (1)

ORR at cathode: $O_2 + 4H^+ + 4e^- \rightarrow 2H_2O$ (2)

Overall reaction: $2H_2 + O_2 \rightarrow 2H_2O$ (3)

A diagrammatic representation of the PEFC is shown below. Centrally located is the membrane electrode assembly (MEA) consisting of an ionomeric membrane, typically Nafion® or other perfluoro sulfonic membranes. Flanking the membrane are two electrodes coated with supported catalyst layers. The electrodes are often specifically textured to allow maximum gas permeation over the whole catalyst layer on the membrane. Flow field plates complete the assembly and serve as current collectors.

Figure 3 - Schematic diagram of (a) typical PEFC and (b) single cell fuel cell (Source: US DOE Fuel Cell Handbook)

The major barrier to commercialisation of PEFCs is the high intrinsic cost of Pt. This has resulted in much research being aimed at lowering the Pt loading, or optimising it. The goal of lowering Pt loading in the PEFC catalyst layers can be achieved through various methods. While some groups have created highly complex dendritic Pt structures [11, 12], others have focused on improving the order of Pt and support atoms in the catalyst layer [13, 14] . Core-shell structures [15] have also been explored to maximise the available surface area of Pt nanoparticles. Another method that has been tested is to improve the porosity of the support materials to allow better Pt dispersion and thus more effective utilisation of the catalyst. Support materials (traditionally carbon black or high surface area carbonaceous materials) serve to provide an electrical contact to the catalyst. Other selection criteria for the support material include high porosity to maximise the coverage of catalyst, good surface adhesion for the catalyst to prevent aggregation and catalyst dissolution, and good structural strength and integrity. Without an electronically conductive support material, electron transfer will not occur from the catalyst layer and the fuel cell would be rendered useless.

2.0 Literature Review

The role of surfactants in stabilising suspended nanoparticles is indisputable. In the past decade, numerous studies with surfactants have resulted in irrefutable evidence of reduced nanoparticles aggregation, increased steric stabilisation and better nanoparticle dispersion in solutions. Aiken & Finke's review in 1999 distinguished surfactant stabilisation via three modes: steric, electrostatic and electrosteric [16].

As such, the role of surfactants has been studied in great depth on several fronts including gold nanorods for biomedical applications [17], controlling aggregation of spherical silver sols for improved SERS activity [18], development of new magnetic resonance imaging (MRI) contrast agents [19] and nanoparticles as drug delivery mediums [20]. Of course, many more examples of surfactant investigations can be cited; however, the interest of this paper is solely for fuel cells, which will be the focus henceforth.

Fuel cells require nano-scale catalysts with high specific surface areas in order to function effectively. Since the most suitable catalyst for fuel cells is Pt (extremely costly), it is even more vital that the size requirement is met to maximum the specific surface area while lowering the Pt loading. Nanoparticles, however have the tendency to agglomerate due to high specific surface energies [6 - 8]; furthermore, the smaller the nanoparticle the higher the specific area and the higher tendency to agglomerate [21]. Stabilising nanoparticles has therefore been the subject of many works and is the prospective role for surfactants, as is highlighted below.

In 1994, Yonezawa et al. [24] presented the case of non-ionic surfactants protecting platinum (Pt) nanoparticles; their investigation used a nuclear magnetic resonance (NMR) technique.

They also proposed a possible model of Pt-surfactant interaction: the hydrophobic portion of surfactants adsorbing strongly to the Pt cluster, leaving the hydrophilic ends trailing into the water (Figure 4). Shortly afterwards, Tanori et al. [25] showed that Pt metal colloids obtained by chemical reduction are well stabilized by some surfactants that prevented aggregation.

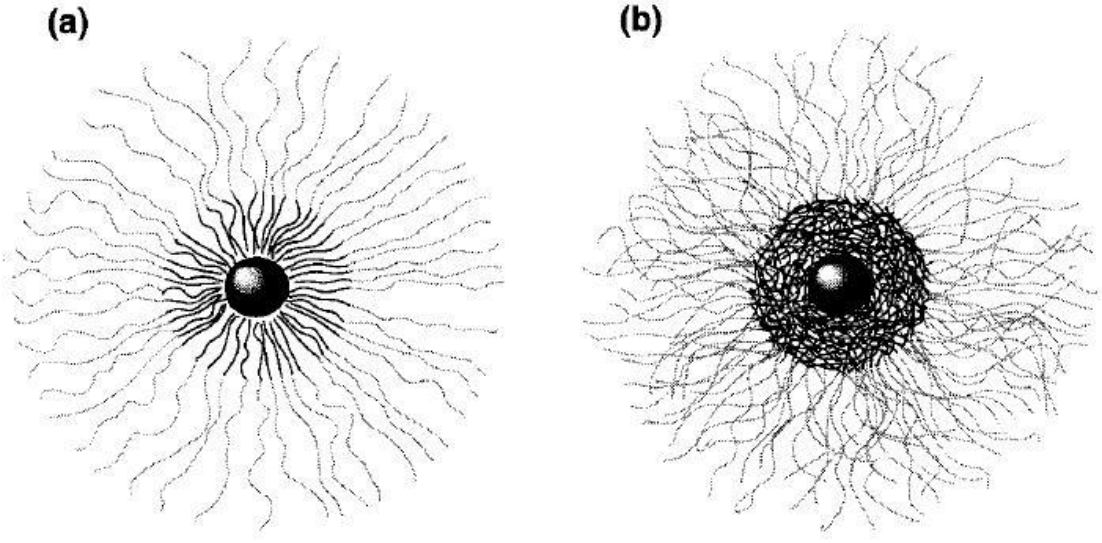

Figure 4 - Schematic illustration of the model of surfactant protected Pt clusters (a) Pt cluster embedded in the hydrophobic domain of the micelle, and (b) Pt cluster adsorbed by the alkyl parts of the molecules on its surface (Source: Yonezawa et al. [24]**)**

Wang et al. [26] later documented the use of dodecyldimethyl(3-sulfo-propyl)ammonium hydroxide (SB12) surfactant in the synthesis of Pt and Pt/Ru catalysts to prevent colloid aggregation in polymer electrolyte membrane fuel cells. Their work showed that the alcohol reduction pathway used did not influence the binding/dispersion of the metal colloids to the carbon support. Furthermore, their findings supported that of previous work done by Bonnemann et al. [27] in claiming that the surfactant had a negligible effect on the activity of Pt.

Works by Lim et al. [28] and Hui et al. [29] showed that the use of surfactants also promoted the optimum Pt particle size between 2-3nm using different types of surfactants. The former presents evidence that mixtures of non-ionic and anion surfactants result in less compact micelles, which directly influence the Pt particle size. Hui's study further included surfactant removal methods; they suggested that an ethanol wash protocol was sufficiently effective in removing the SB12 surfactant used. Samples washed using this method were tested electrochemically and were comparable to commercially available E-TEK catalyst of similar weight percent. The molar ratio of surfactant to Pt precursor was also emphasised, as it appeared to directly affect the average particle size and size distribution of Pt nanoparticles. This was previously also shown by Chen et al. [30] albeit with gold nanoparticles.

It was reported by Hong et al. [31] that the use of a novel amphiphilic surfactant tergitol phosphate in fuel cell electrodes showed improved performance. Their novel surfactant yielded two specific benefits: Firstly, in the promotion of triple phase boundaries within the catalyst layer using the hydrophilic and hydrophobic regions to conduct the liquid and gaseous phases respectively; also, the surfactant appeared to have a dispersing effect and promoted a more uniform Pt/C distribution in the electrode.

In 2009, Wills et al. [32] from the University of Southampton reported the use of 4 different fluorocarbon surfactants in the manufacture of inks and ionomer components of a PEM fuel cell. Their study found that surface wetting of carbon paper supports and PTFE surfaces are increased. Also the anionic surfactant leeched into water, ionomer and methanol solutions, an unacceptable outcome.

The studies cited above indicate that the use of surfactants in various aspects of fuel cell manufacture have been tried and tested with mixed results. Often an improvement in performance is accompanied by negative impacts in other areas. This study examines the impact of Tergitol NP-9 surfactant on catalyst performance. Further comparisons are also made with one commercial catalyst, and another catalyst utilising graphene oxide (GO) as support. The latter is reviewed here below.

Although only recently exposed as a material with tremendous potential in various applications, graphene and its derivatives have already been investigated for use as catalyst supports in fuel cell applications.

Seger and Kamat [33], in 2009, showed prepared Pt nanoparticles supported on graphene sheets by reducing borohydrides in a graphene oxide suspension. They then implemented these Pt catalysts into fuel cells and obtained a maximum power of 161mW/cm^2 as compared to 96 mW/cm^2 for the unsupported Pt fuel cell. Li et al. [34] and Ha et al. [35] also showed in separate studies that Pt nanoparticles supported on graphene produced slightly better ORR activity than conventional Pt on carbon supports.

Jung et al. [36] fabricated Pt/C hybrid catalysts with GO and made some interesting discoveries. Firstly, GO appeared to improve the durability of the catalyst. They attributed this electrochemical stability to the high carbon crystallinity of Pt/GO. Although the hybrid catalysts showed lower initial electrochemical currents in an MEA, it recorded an activity loss of only 17.7% as compared to 45.4% in the commercial Pt/C catalyst. Their findings led them to suggest that GO prevents Pt agglomeration by providing an anchoring site of eluted metal.

Park et al. [37] highlighted the loss of active sites in Pt/graphene catalysts due to the horizontal stacking of the 2D graphene sheets. They therefore doped Pt/graphene catalysts with carbon black at various concentrations, and these carbon particles acted as a spacer in between the graphene sheets. Their results indicated that the catalyst-ionomer interface increased with the amount of carbon black added into the catalyst layer. However, the maximum ECSA and faster interfacial oxygen kinetics were obtained at 25 wt.% carbon black loading.

In another example of hybridisation, glucose was carbonised in situ on the surface of Pt/graphene catalysts. This work, performed by Liu et al. [38], showed via chronoamperometric methods that the hybrid Pt/graphene-C catalyst exhibited similar catalytic activity but up to four times better stability over long durations. This enhanced stability was attributed to the effect of carbonisation in preventing Pt nanoparticle agglomeration.

Much focus has also been given to nitrogen-doped graphene. In 2009, Groves et al. [39] reported on the improved binding energy of Pt to graphene achieved with nitrogen doping. Although no electrochemical tests were performed in this study, it could be inferred that increase bond strength between Pt and graphene implied less Pt dissolution or dislodgement and would translate to better performance in a fuel cell. A more relevant study by He et al. revealed that nitrogen-doped graphene oxide supports exhibited better catalyst activity and lower losses of ECSA than commercial Pt/C catalysts as well as regular Pt/GO [40]. This finding was confirmed by several works [41 – 44], among which also report increased CO tolerance[42] and preference towards the four electron pathway to form water [42, 43].

3.0 Aims & Objectives

The aim of this study was to evaluate the potential of certain novel PEFC supports - surfactant additives and reduced graphene oxide (rGO) supports - on the performance of the catalyst ink for application in a PEFC MEA or membrane electrode assembly. *Ex situ* electrochemical characterisation was performed to assess the catalyst suitability for both the HOR and ORR reactions. The durability of these catalyst inks was also examined to assess the long term performance and reliability of the catalyst.

In order to accomplish these aims, cyclic voltammetry (CV) was used to evaluate the Electrochemical Surface Area (ECSA), a measure of the available Pt catalyst surface area. Besides CV tests, the samples were also evaluated for mass and specific activity. Linear sweep voltammetry (LSV) was then used to assess catalyst activity. Finally, accelerated degradation testing (ADT) was used as a means to test the durability of the catalyst under cyclic loads, replicating the conditions of the actual application in a fuel cell.

As both novel catalysts were prepared with completely different methods, a benchmark was required against which the performance of the novel catalysts could be compared. For this purpose, the commercially available Tanaka TEC10E50E 45.9 wt. % Pt/C (TKK) was chosen. The TKK catalyst is of the highest quality and is widely used Pt/C catalyst for research and commercial purposes.

4.0 Experimental

4.1 Scope of work

In this work, two different methods of optimising Pt loading were explored. The first method involved the use of surfactants in the fabrication of Pt catalyst ink. Surfactants have been shown to prevent agglomeration of metallic nanoparticles in numerous applications and even improve fuel cell performance [16-18]. A variety of commercially available surfactants were initially screened such as Tergitol® - Type NP-9 Nonylphenol Ethoxylate (NP9) and Cetyl Trimethyl Ammonium Bromide (CTAB). However, preliminary work with CTAB uncovered a major obstacle: CTAB formed non-soluble precipitate in the perchloric acid ($HClO_4$) electrolyte and as such was expected to negatively impact the catalyst when prepared as an ink. Also, available literature has indicated an extent of bromide ion poisoning on Pt catalysts [47, 48] that severely deteriorates its performance.

The second method employed the use of graphene oxide (GO) as the choice support material for the Pt nanoparticles. Graphene has received much attention lately due to its exceptionally high crystal and electronic quality [49], lending it a versatility for numerous prospective applications [36 – 38]. Not surprisingly, it has also been considered as support material for PEFCs, whether as the sole support material [34, 39], or in tandem with other existing support materials [39 – 41]. Some works have claimed a higher CO tolerance in Pt catalysts supported on graphene nanosheets [42, 43]. In this work, GO was synthesised using Hummer's method and used directly in place of activated carbon.

The electrochemical experiments were performed using an Autolab potentiostat with a linear scan module connected to a Pine rotator control device.

4.2 Experiment setup

An electrochemical glass cell was filled with 100ml of 0.1M perchloric acid electrolyte. The cell was then placed onto its stand in the Faraday cage. Inlet and outlets for the water jacket were connected; the water bath was then switched on and set to 25°C. This setup utilises three separate electrodes (which will be described in detail following this section).

The counter electrode and the reference electrode were prepared, installed to the cell and connected to their respective electrical terminals.

The working electrode was then installed to the shaft of the rotator and lowered into the electrolyte carefully. As a general rule of thumb, all three electrodes were put at the same level for consistency in measuring ohmic resistance later. Having the reference and counter electrodes at a slightly higher position than the working electrode also ensured more smooth convection during the ORR experiments.

The gas feed (nitrogen first, oxygen later) was then inserted into the cell, below the electrolyte surface. The gas pressure was set to between 1 - 1.5 bar on the cylinder and the needle valve to 1.5-2 mm. It was important to ensure the gas did not bubble too deep into the electrolyte as it risked bubbles getting trapped in the reference electrode or on the working electrode, both of which would negatively affect the experiment. For example, a bubble trapped at the tip of the reference electrode could disrupt the continuity of the solution in the electrode and in the cell resulting in exceedingly high potentials being cycled by the potentiostat causing irreparable carbon corrosion on the working electrode.

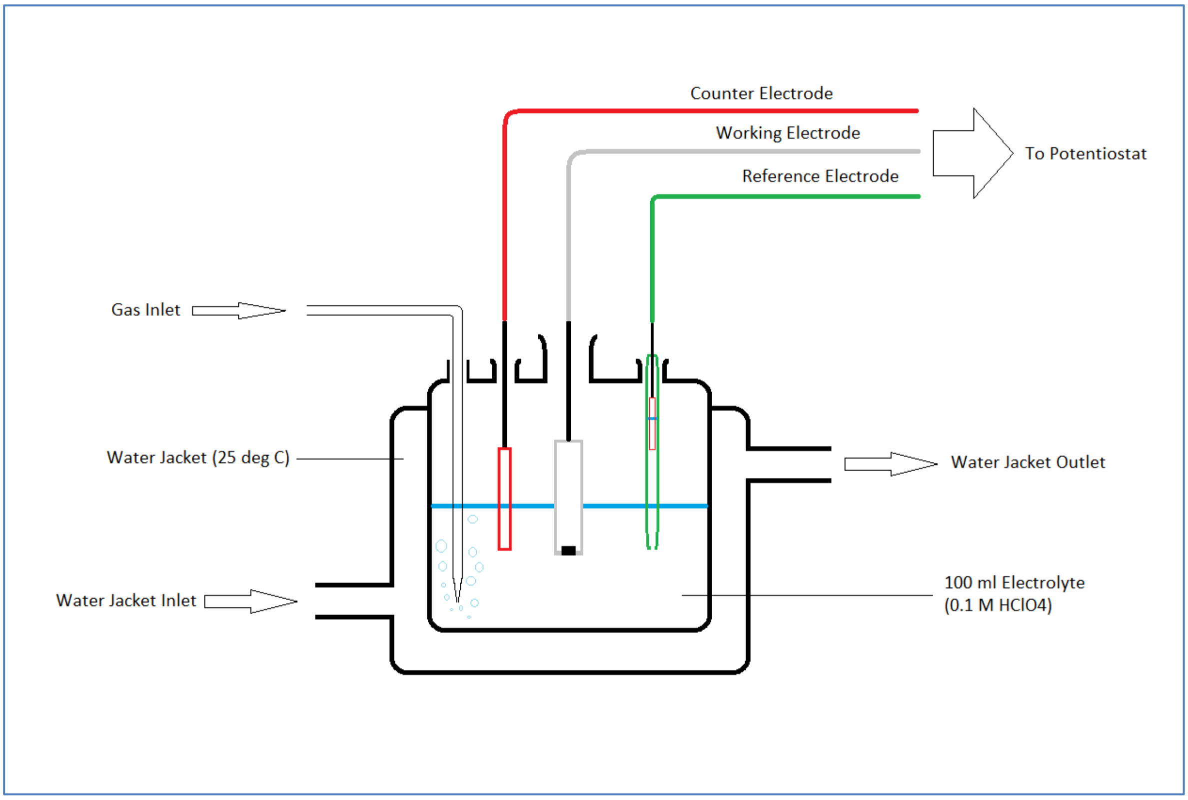

Figure 5 - Schematic of electrochemical cell setup

4.2.1 Counter electrode

The counter electrode used was a self-assembled platinum wire wrapped with platinum gauze. Using Pt gauze increased the available surface area. The counter electrode was rinsed with Ultra High Quality (UHQ) 18.2 Millipore water before every use and also flamed until the surface glowed red. This was especially important in the use of surfactants; they were not easily rinsed out with water from the gauze, hence the flaming to eliminate all traces of impurities.

Figure 6 - Counter electrode affixed with a rubber stopper to maintain an airtight connection with the electrochemical cell

4.2.2 Reference Hydrogen Electrode

The reference hydrogen electrode (RHE) used in the electrochemical was self-made. It incorporated a short length of platinum gauze suspended from a wire, encased in a short glass pipette sealed around the wire and with a small hole at the bottom (Figure 7)

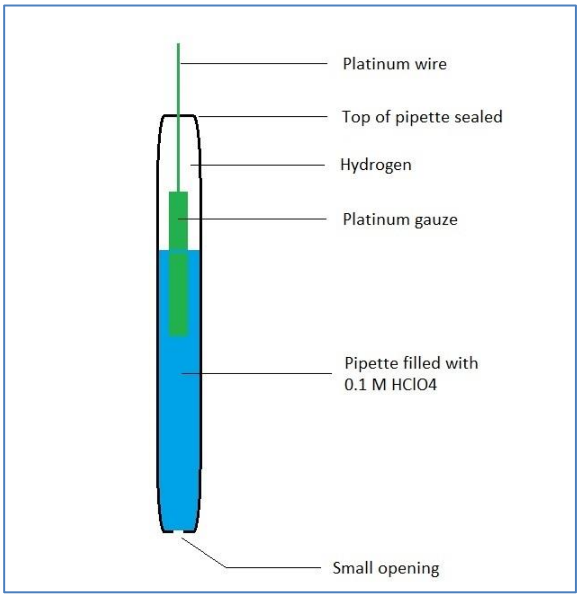

Figure 7 - Schematic of self-made Reference Hydrogen Electrode (RHE)

The pipette was then filled with UHQ water using a syringe, to check for leaks in the upper sealed area around the wire. As hydrogen was to be used in the RHE, no leaks were acceptable and the hole at the bottom also had to be small enough to cause a capillary effect within the RHE. If both these conditions were fulfilled, any liquid trapped inside would not flow freely out.

The water was then shaken out carefully and the RHE stored for future use.

However, it was noted that any material that was entrained in the electrolyte of the cell would also be trapped in the RHE (since a continuous system was expected). As such, the RHE was broken and remade every month or after about 50 cycles of use, whichever point was achieved first.

Charging and Installing the RHE

The RHE was charged by filling the upper space with hydrogen. A syringe (Luer 2ml from BD Plastipak) affixed with a 21G needle (Terumo) was first used to fill the RHE with perchloric acid; all air bubbles were released by gently tapping on the side as the RHE was filled.

When the RHE was filled, it was then placed in a beaker of perchloric acid and connected to the negative terminal of a power source (Manson). The positive terminal was attached to a separate platinum wire, and also placed into the beaker. When the power source was switched on to approximately 15V, hydrogen was produced via electrolysis on the platinum gauze within the RHE and rose to occupy the upper space of the sealed RHE.

The power source was switched off when the hydrogen displaced the perchloric acid approximately halfway down the platinum gauze. The RHE was then transferred to the electrochemical cell with care to ensure no air bubbles entered the RHE or were trapped at the bottom opening - the perchloric acid in the RHE should be a continuous system with the electrolyte in the cell.

4.2.3 Working Electrode

The working electrodes were obtained from Pine Instruments (USA). The working electrodes for rotating disk voltammetry were a glassy carbon disk of 5 mm in diameter. The electrodes were suitable for working temperatures up to 40 °C and not reliable for high temperature studies.

Polishing

Electrodes were polished on Buehler Polish Paper with Alumina paste of 1.0, 0.3 and 0.05 microns. The electrodes were rinsed with UHQ water in between each size step. After polishing, the GCEs were sonicated in the ultrasound bath for up to 1 minute to remove all traces of the alumina polish. Different polish paper was used for each paste size and a different set of polish paper was used for the polycrystalline Pt disc and GCE respectively. This was to prevent cross contamination i.e. Pt particles deposited from the GCE onto the polycrystalline Pt disc.

Before the application of ink onto the GCE, the electrodes were dried thoroughly. While drying in a vacuum oven ensured quick drying, water stains were sometimes observed on the glassy carbon surface. An alternative method of blowing nitrogen onto the electrodes ensured complete drying with no such water stains. A schematic for this setup is shown below.

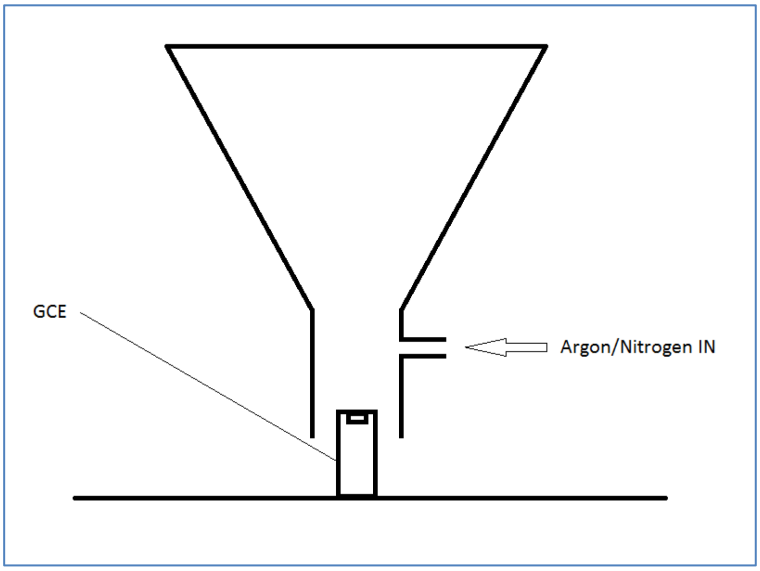

Figure 8 - Setu for blowing dry GCEs before ink application

A thoroughly dry electrode is evidenced by high hydrophobicity of the teflon area around the glassy carbon surface - when the ink is dropped onto the electrode surface it forms a droplet that does not easily spill into the teflon area while the actual shape/profile of the droplet is related to the functional groups present in the ink.

Ink Application & Drying

The amount of ink applied onto the electrode surface depended on the intended loading. However, the area of the electrode surface also limited the amount of ink that could be applied. As a general rule, the 5mm diameter electrode could accommodate up to 15µl of ink. It should also be noted that the more ink applied, the longer the resulting drying time and the more care required for drying to avoid the droplet spilling off the glassy carbon surface of the electrode.

Several methods of drying were tested. Garsany et al. noted countless observations of inappropriate drying methods, categorised by imperfect ink films that were subsequently formed [56]. As electrochemical testing of these films very much relied on surface area measurements which in turn depended heavily on the accessible surface area of Pt nanoparticles, this aspect of preparation was of great importance for producing good and reproducible ink films.

One effective method was to drop 2µl of ethylene glycol (EG) on top of the ink droplet. The electrode was subsequently rotated on axis at up to 200 rpm for approximately 20 minutes to promote complete ink coverage before further oven drying at 40°C. This method proved effective for preventing the 'coffee ring stains' that were often observed from stationary drying. EG is highly viscous and served to slow down the rate of evaporation of liquids from the ink droplet, thus enabling more uniform drying at the expense of far longer drying times (up to 18 hours in some cases).

Another effective method was similar, but without the use of EG. Once the ink was applied onto the electrode, it was spun under cover for approximately 30 minutes. After this time (by which the droplet had also partially dried into a flatter surface), the electrode was placed in the vacuum oven at 40°C and approximately 800 mbar pressure. The electrode would be ready for testing in less than 6 hours through this method.

4.2.4 Electrochemical Cell & Glassware cleaning

Electrochemical testing requires all glassware to be free of impurities and contaminants. These contaminants may be present in the air, on surfaces or even in water. As such, a rigorous cleaning procedure was used to ensure the highest possible level of sterility for all glassware.

When washing glassware, only fresh UHQ milipore water was used. Furthermore, all clean glassware was stored separately with nozzles and openings wrapped in aluminium foil. To prevent contamination from the air, glassware was also filled with UHQ water where possible before storage.

An acid bath soaking method was used to clean all glassware before experiments. This was typically done the day before experiments and involved a 2 stage process.

Glassware - Acid soak

A solution of concentrated nitric and sulphuric acids was prepared in a 1:1 volumetric ratio.

The glassware items that require cleaning were put into a glass basin; the basin placed on a heating plate. The acid solution was then poured over the glassware (and into it where possible) to expose all surfaces to the acid for cleaning. Once a sufficient amount of acid had been poured out onto the glassware, the heating plate was switched on to approximately 80 °C. The acid soak was left for 2 hours. This step could also be done without the use of a heating plate – the acid soak was then left overnight.

Following the acid soak, the basin was removed from the heating plate and left to cool for several minutes. Items were removed from the acid before rinsing thoroughly with UHQ water.

The glassware was rinsed several times and shaken vigorously to eliminate all traces of the acid mixture before filling with UHQ water and covering the outlets with foil. The glassware was cleaned as close as possible to the time of use to minimise contamination.

Teflon and plastic components – Ultrasound bath or Piranha solution

Some glassware had Teflon or plastic accessories and fittings (eg. caps for measuring flasks). These could not be cleaned using the acid soak, especially with heating as it would have caused damage. A simple method for cleaning these components was to soak them in UHQ water in a clean beaker and irradiate in an ultrasound bath for several minutes.

Alternatively a piranha solution can be used for this purpose, or also for quick effective cleaning (where an overnight acid soak would not be practical). The piranha solution consisted of concentrated sulphuric acid with hydrogen peroxide in an approximately 2:1 volumetric ratio. The procedure for this cleaning method involves putting the Teflon pieces into sulphuric acid and hydrogen peroxide. Because of the highly oxidative nature of hydrogen peroxide, it was topped up slightly before every use. This method was also carried out in a water bath due to the highly exothermic nature of peroxide in action. Soaking the Teflon components for approximately 30 minutes was sufficient.

4.3 Preparation of Catalyst Ink

All Pt/C inks made were customised to provide a loading of 20 µg/cm^2 when dropped onto a 5 mm diameter glassy carbon electrode. Three types of catalyst ink were made and tested:

a) Pt/C with NP9 surfactant

b) Pt/GO

c) Pt/C using commercial TEC 10E50E Pt catalyst

4.3.1 Pt/C with NP9 surfactant

The steps below were provided by Dr Jill Newton, who kindly supplied the information and some samples for electrochemical characterisation used in this work.

Preparation of Pt nanoparticle suspension

All glassware was cleaned with aqua regia (concentrated nitric acid and hydrochloric acid mixture at 1:3 ratio) and then rinsed thoroughly with ultra-high quality (UHQ 18.2 mΩ) water prior to use. 1.95 ml aged K_2PtCl_4 1% aqueous solution (Sigma Aldrich 99.9%), and 4.58 ml NP-9 Tergitol (Sigma Aldrich) were added to 73.2 ml UHQ water in a round-bottomed flask.

The mixture in the flask was then stirred at 600 rpm using a magnetic stirrer while being heated to 70°C for 4 hours, after which the initially clear solution would turn black. The fine particle sizes produced negated the use of conventional filtration methods. As such a purification process of the colloidal Pt with centrifugation and re-dispersion was employed.

The dispersion was first centrifuged at 26 000 rpm and 10°C for 20 minutes in a Sigma 3K30 refrigerated centrifuge. The supernatant was then discarded and the precipitate re-dispersed in UHQ water. This re-dispersion step was repeated three times.

The concentration of Pt in the final dispersion, determined via Thermo-Gravimetric Analysis was found to be 0.22 wt%.

Preparation of Pt catalyst ink

A stock solution was prepared with 9.88 g UHQ water, 0.02 g Nafion 10% and 0.004 g Vulcan XC72.

The stock solution was sonicated in an ultrasound bath for approximately 45 minutes to ensure a good dispersion of the carbon particles in the solution. From the stock solution, 0.84 g was weighed out in a new, clean sample vial and added with 0.16 g of the colloidal Pt nanoparticle dispersion. From this preparation, 11.5 µl of ink dropped onto a 5 mm glassy carbon electrode would give a loading of 20 $\mu g/cm^2$.

4.3.2 Pt/GO

Graphene oxide (GO) was used as catalyst support in place of the typical Vulcan XC72 support. The highly oxidised graphene was produced using Hummers' method (1). Polyol synthesis using a microwave facilitates the reduction of GO and the simultaneous attachment of Pt nanoparticles.

Preparation of Pt/GO nanoparticles

Three solutions were prepared separately. The first solution was 0.04 g GO in 20 ml ethylene glycol (EG) sonicated for 70 minutes. The second was 0.4 ml of 0.4 M potassium hydroxide (KOH) in de-ionised (DI) water and finally 1 ml of 0.05 M potassium hexachloroplatinate (K_2PtCl_6) in DI water.

These three solutions were mixed together and sonicated for 60 minutes. After sonication, the mixture was put into a large beaker and microwaved for 50 seconds at 300W; the large beaker ensured no spillages as the solution would boil aggressively during microwave treatment. Microwave treatment produced a black precipitate indicating the reduction of GO; the mixture was then cooled. After cooling, the solution was centrifuged at 3000 rpm for 30 minutes, following which the supernatant was discarded. The precipitate was then re-dispersed with acetone and centrifuged again with the same settings as before; this step was repeated three times. Finally, the remaining precipitate was dried in a vacuum oven overnight at 50°C and under 800 mbar vacuum; the weight of the dried precipitate was later measured to calculate the yield.

Preparation of Pt/GO catalyst ink (adapted from literature; see following section)

1.96 mg of Pt/GO dried catalyst was weighed out in a clean sample vial. 1.15 mg of UHQ water was added carefully (to prevent the nanoparticle powder from being aerated). Following that, 0.27 mg of iso-propyl alcohol (IPA) was added to the mixture. Finally, 1μL of Nafion 10% solution was added. The mixture was shaken and then sonicated for 30 - 45 minutes to ensure good nanoparticle dispersion in the ink solution.

4.3.3 Pt/C from commercial TEC 10E50E Pt catalyst

The commercial catalyst obtained from Tanaka Kikinzoku International K. K. (TKK Pt/C) was used in this preparation. The Pt weight content is 45.9 wt. % on high surface area carbon support. This commercial product is known as a highly dispersed quality catalyst with high performance and durability.

The ink preparation formula was adapted from literature as used by Takahashi and Kocha [57]. The steps are given below are for the preparation of 1.5 ml of catalyst ink. 1.28 mg of Pt catalyst (TEC 10E50 45.9 wt. %) was weighed out in a clean sample vial. 1.15 mg of UHQ water was added carefully (to prevent aeration of the Pt nanoparticles). Following that, 0.27 mg of iso-propyl alcohol (IPA) was added to the mixture. Finally, 1μL of Nafion 10% solution was included in the mixture.

The ink was shaken and then sonicated for 30 - 45 minutes to ensure good nanoparticle dispersion in the ink solution.

4.4 Experimental Procedures

4.4.1 Autolab GPES Procedures for CV and ORR tests

Measurement of Open Circuit Potential

The Open Circuit Potential (OCP) refers to the background voltage of the cell when no work is performed. Later, all results obtained are considered with respect to the Open Circuit

Potential. It was measured using the chronopotentiometry method of measuring potential over time at a zero current while gas was bubbled into the solution. The gas bubbled through the system depended on the phase of the test; for CV measurements, the electrolyte was purged with nitrogen to remove all traces of oxygen to simulate the HOR reaction of the PEFC whereas oxygen was used for the LSV measurements to simulate the ORR reaction of the PEFC. It was found that at the bubbling conditions specified previously, the system took about 20 to 30 mins to reach saturation point. This was confirmed by the plateau in potential after 20 mins. The typical OCP value was between 0.8 V and 1.0 V when the solution was deoxygenated and was slightly higher (0.9 - 1.1 V) when bubbled with oxygen.

Conditioning of Pt active sites

Prior to measuring the Electrochemical Surface Area (ECSA) of the ink samples, the ink films were conditioned to optimise and uncover the Pt surface on the supports. This was done by cycling the voltage rapidly at scan rates of 250 mV/s or higher between 0.05 – 1.1 V for in excess of 100 cycles, resulting in greater exposure of Pt active sites leading to higher ECSA values measured later.

Cyclic Voltammetry to Enumerate ECSA values

Cyclic voltammetry was used to evaluate the ECSA of the catalyst ink. The ECSA is generally used as a baseline indicator for catalyst performance because it provides basic information on the availability of active Pt sites for catalysis. To effectively measure the ECSA, cyclic voltammetry was performed at low scan rates (≤ 20 mV/s, 3 cycles) to obtain a cyclic voltammograms. The ECSA value is calculated using the area under the Hydrogen underpotential desorption peak and is given using the formula below:

$$ECSA\left(\frac{m^2}{g_{Pt}}\right) = \frac{Q_{Hupd} \times 100}{A \times L \times Q_H} \qquad (4)$$

Where, Q_{Hupd} is charge (µC) given by the area under the hydrogen underpotential desorption peak, A is the geometric surface area (cm^2), L is the Pt loading on the electrode (mg/cm^2) and Q_H is the charge required to oxidise one monolayer of hydrogen on the Pt surface (210 $\mu C/cm^2$).

Figure 9 shows a characteristic CV for commercial Pt/C inks. The value of Q_{Hupd} in Equation (4) is taken as the area under the hydrogen underpotential desorption peak, OR the average area between the hydrogen underpotential desorption and adsorption peaks.

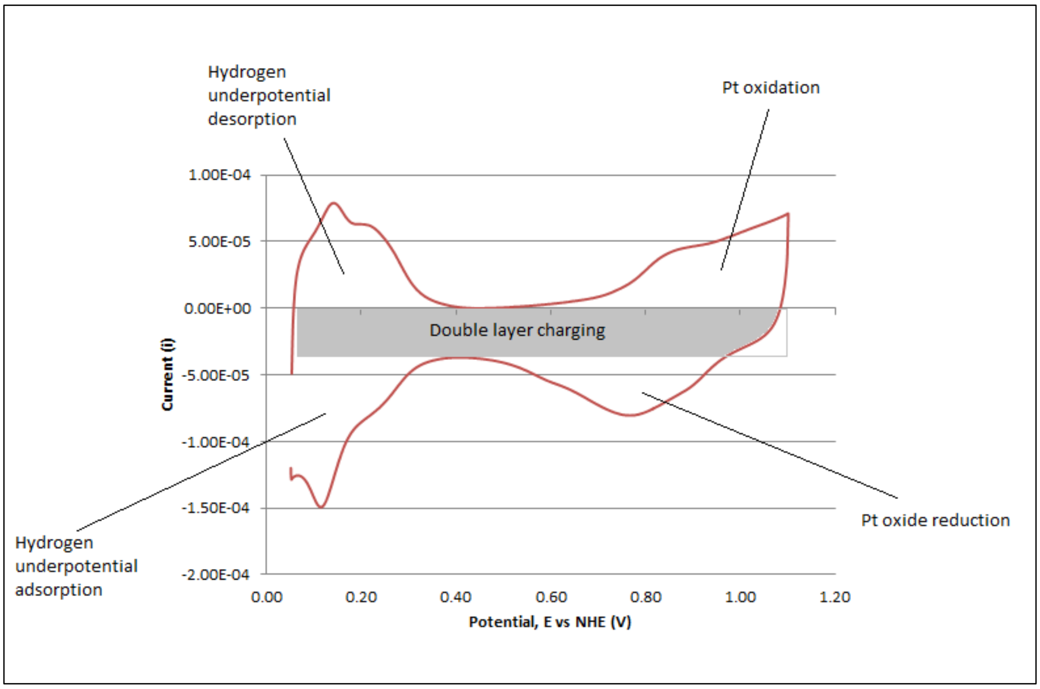

Figure 9 - Characteristic regions of a cyclic voltammogram for Pt

Linear Sweep Voltammetry and ORR activity

The linear sweep voltammetry (LSV) method was used to evaluate the catalyst activity. It has been well established that the rate limiting step in a PEFC is the ORR reaction, at six or more orders of magnitude slower than the HOR [58]. As such, evaluation of catalyst activity is a vital step towards improving the catalytic performance for the ORR. The catalyst activity was evaluated using the rotating disk method.

The GCE is rotated at fixed speeds to induce hydrodynamic flow of the electrolyte towards the ink film. By controlling the rotation speed, the convection effects can be controlled correspondingly and incrementally, thus allowing for the isolation of kinetic effects when evaluating the combined effects of kinetics and mass transport. The rotation speeds used in this study were 400, 800, 1200, 1600 and 2000 rpm respectively, while the scan rate for the LSV sweeps were 10 mV/s. The Levich equation provided the theoretical data for the ORR performance to be compared and used alongside the experimental data. The Levich equation is as follows:

$$I_L = (0.620)nFAD^{0.67}\varpi^{0.5}v^{-0.17}C \qquad (5)$$

Where, I_L is the mass-transport limiting current (A), n is the number of electrons transferred in the half reaction, F is the Faraday constant (9.649 X 10^4 C/mol), A is the geometric surface area (cm^2), D is the diffusion coefficient (cm^2/s), ϖ is the angular velocity of the electrode (rad/s), v is the kinematic viscosity (cm^2/s) and C is the electrolyte concentration (mol/cm^3).

The mass and specific activities were calculated from the LSV curves, by utilising the kinetic current as a starting point. The kinetic current may be obtained by extrapolating the curves at various rotation speeds in the Koutecky-Levich plot (i^{-1} vs $\omega^{-0.5}$) to infinite rotation speeds, or through the following equation:

$$i_k = \frac{i_{lim} \times i}{i_{lim} - i} \qquad (6)$$

Where i_k is the kinetic current (A), i_{lim} is the measured limiting current and i is the current measured at the potential used for evaluation of ORR kinetics [59].

From Equation (6), the mass activity is calculated by normalising to the Pt loading:

$$i_m = \frac{i_k}{Pt\ loading} \qquad (7)$$

Where i_m is the mass activity (A/mg), i_k is the kinetic current (A) and the Pt loading has (mg) units.

Simultaneously, the specific activity can also be calculated using the following equation:

$$i_s = \frac{i_k}{(\frac{Q_H}{210\ \mu Ccm^{-2}})} \qquad (8)$$

Where i_s is the specific activity (µA/cm^2), i_k is the kinetic current (A) and Q_H is the charge (C) given by the area under the Hydrogen underpotential desorption peak.

Impedance Analysis

The *Electrochemical Impedance Spectroscopy* analysis was useful to evaluate the ohmic resistance of the system. Ohmic resistance is also known as solution resistance and is loosely characterised by the resistance to conductivity that is caused by the distance between the working electrode and reference electrode. In some electrochemical setups, the ohmic resistance is minimised by the use of a Luggins capillary reference electrode that is positioned very close to the surface of the ink film.

In this setup, a regular reference electrode was used and the ohmic resistance was calculated and the value used to correct the LSV curves before further analysis.

Accelerated Degradation Tests

The final test for the ink samples was an accelerated degradation test to evaluate the durability of the catalyst. Through square-wave potential cycling between 0.6 V and 1.2 V vs NHE, the Pt surface was repeatedly oxidised (1.2 V) and reduced (0.6V) in excess of 20000 cycles. The

ECSA was measured every 1200 cycles, and plotted in an *ECSA vs Number of Potential Cycles* graph to track the degradation of the Pt catalyst. This was meant to simulate the cycle life of the catalyst as it would be used in a PEFC.

5.0 Results & Discussion

5.1 Cyclic Voltammetry and ECSA

As mentioned previously, the commercial Pt/C catalyst (Tanaka TEC10E50E 45.9 wt. %) was used as the benchmark catalyst for this study. It showed great stability over different scan rates used for performing cyclic voltammetry. The visual observation of the overlapping peak potentials in Figure 10 is indicative of the reversibility of the adsorption of H^+ on Pt.

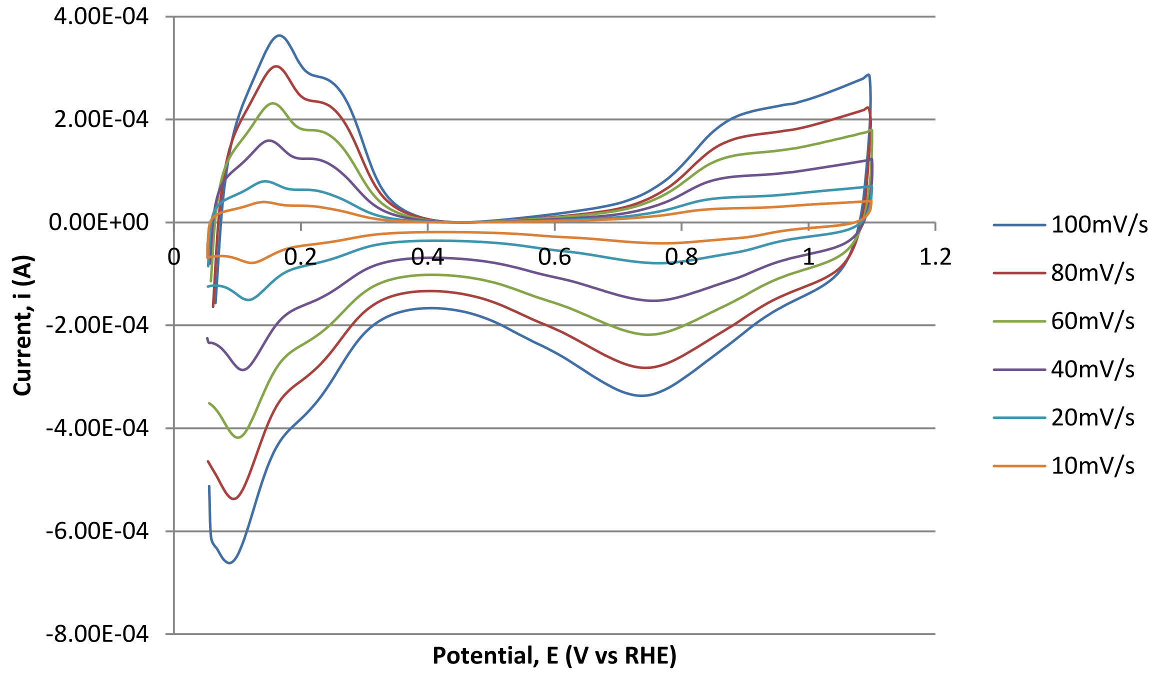

Figure 10 - CVs at different scan rates for TKK Pt/C in deoxygenated 0.1 M $HClO_4$, 25 °C

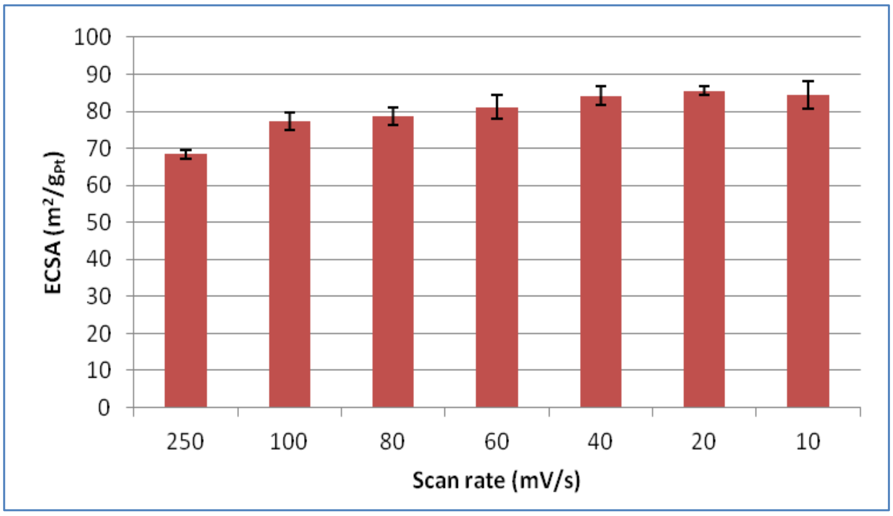

Figure 11 - Average ECSA for commercial TKK Pt/C at various scan rates

Figure 11 shows the ECSA values (calculated using Equation 4) obtained at various scan rates. It is first noted that the highest ECSA values were obtained with a linear scan rate of 20 mV/s. This implied that 20 mV/s was sufficient to maximise the electrical exposure of the Pt active sites.

Also shown in the chart are the standard deviation bars, indicating the range of values obtained over several repeat experiments. Commercial TKK Pt/C shows a high consistency across all scan rates used, validating its selection as benchmark catalyst for this study.

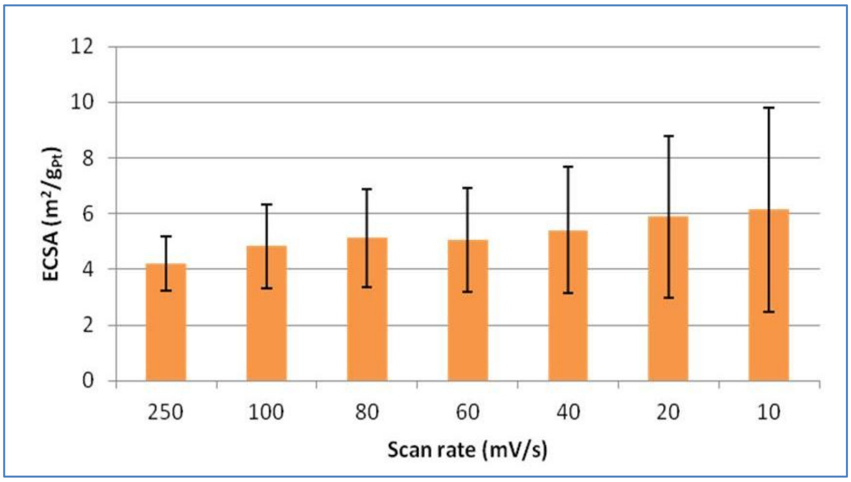

Figure 12 - Average ECSA values for Pt/C NP-9 at various scan rates

As shown in Figure 12, the Pt/C NP-9 catalyst exhibited the lowest average ECSA values across all scan rates, with a notable large variance. Pt-surfactant interactions are the reason for this, especially considering the lack of a surfactant removal step after the reduction of Pt nanoparticles. One study by Cheng et al. [60] noted that the surfactants may obstruct the direct contact between Pt and the carbon support. Since the unanchored Pt contributes no electroactive surface area, this may very well be the reason for the low ECSA values seen, contrary to the findings of Wang et al. [26] and Bonnemann et al. [27] who both noted a negligible impact of surfactant presence on the catalyst activity.

Furthermore, the error bars appear to be widening as the scan rate decreases. This could be a reflection of catalyst inconsistency brought about by the unstable coverage of surfactants on the Pt nanoparticles. Alternatively, natural convection in the electrolyte caused by the concentration gradient in the bulk and electrode interface could also cause the variation in measured ECSA had the test been carried out for extended periods.

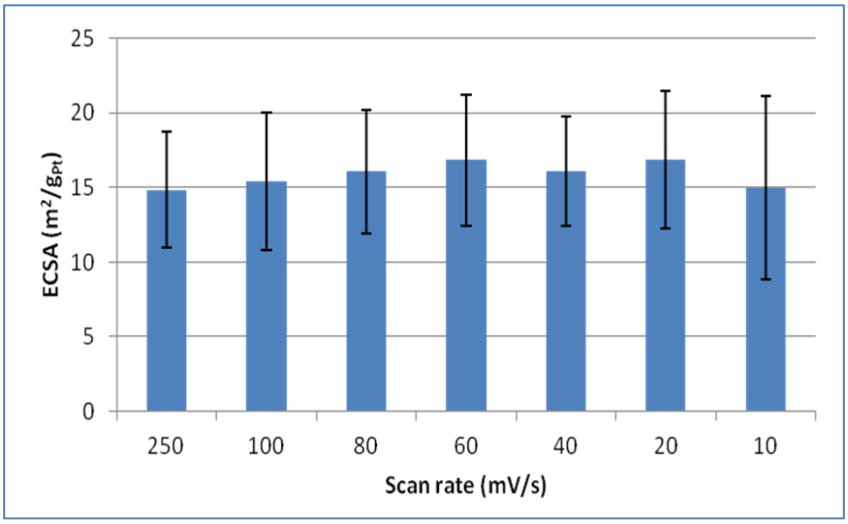

Figure 13 - Average ECSA values for Pt/GO at various scan rates

The Pt/GO catalyst showed intermediary values of ECSA when examined alongside TKK Pt/C and Pt/C NP-9. The trend in Figure 13 suggests that there is not much effect in lowering the scan rate towards the obtained ECSA values. This suggests that the electron transfer proceeds without significant hindrance, implying good conductivity in the catalyst layer.

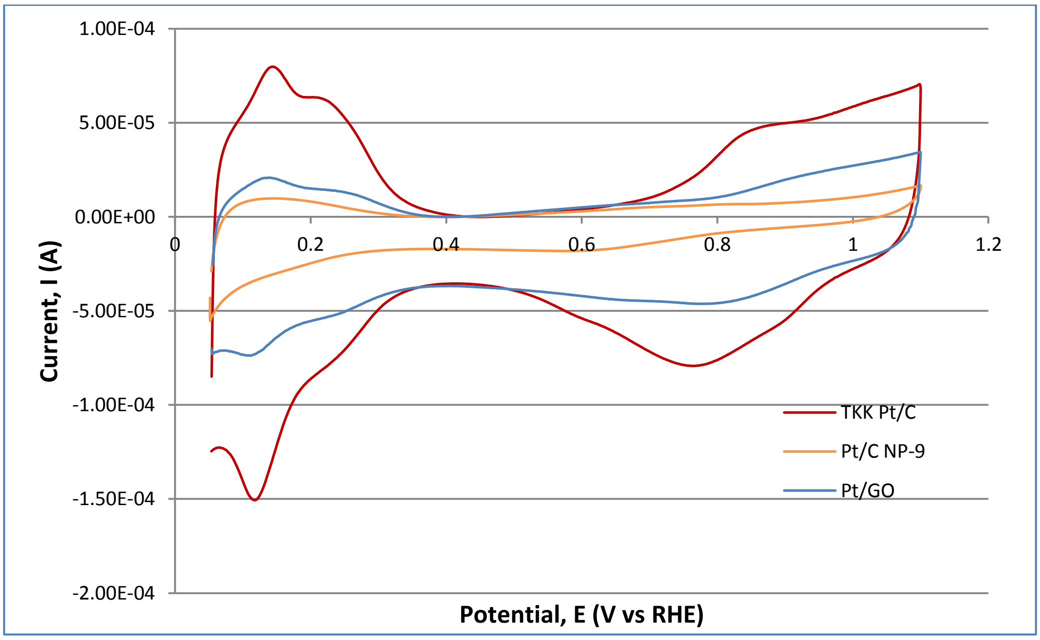

Figure 14 - Overlaid CVs for TKK Pt/C, Pt/C NP-9 and Pt/GO (20 mV/s)

When the CVs for the three catalysts are overlaid (Figure 14), some trends become apparent. Firstly, the double peaks at the Hydrogen underpotential desorption region correspond to the crystal faces of Pt(110) and Pt(100) respectively. These peaks are very apparently in the TKK Pt/C catalyst CV and still discernable in the Pt/GO catalyst CV. However, there is only 1 peak visible for the Pt/C NP-9 catalyst – Pt(110). This could be an indication of the nature of surfactant coverage as surfactant molecules typically orient themselves with the hydrophobic ends towards the metal and hydrophillic tails in the solution. In this respect, the absence of the Pt(100) peak could suggest that it is better shielded than the Pt(110) face.

In Figure 14, the Pt/C NP-9 CV also shows a poorly formed Pt oxidation and Pt oxide reduction region. Once again, this alludes to surfactant shielding of the Pt obstructing access to the Pt sites. The Pt oxide reduction region also appears to be shifted towards a lower potential, indicating some difficulty in accessing the Pt oxide species.

5.2 ORR Catalyst Activity

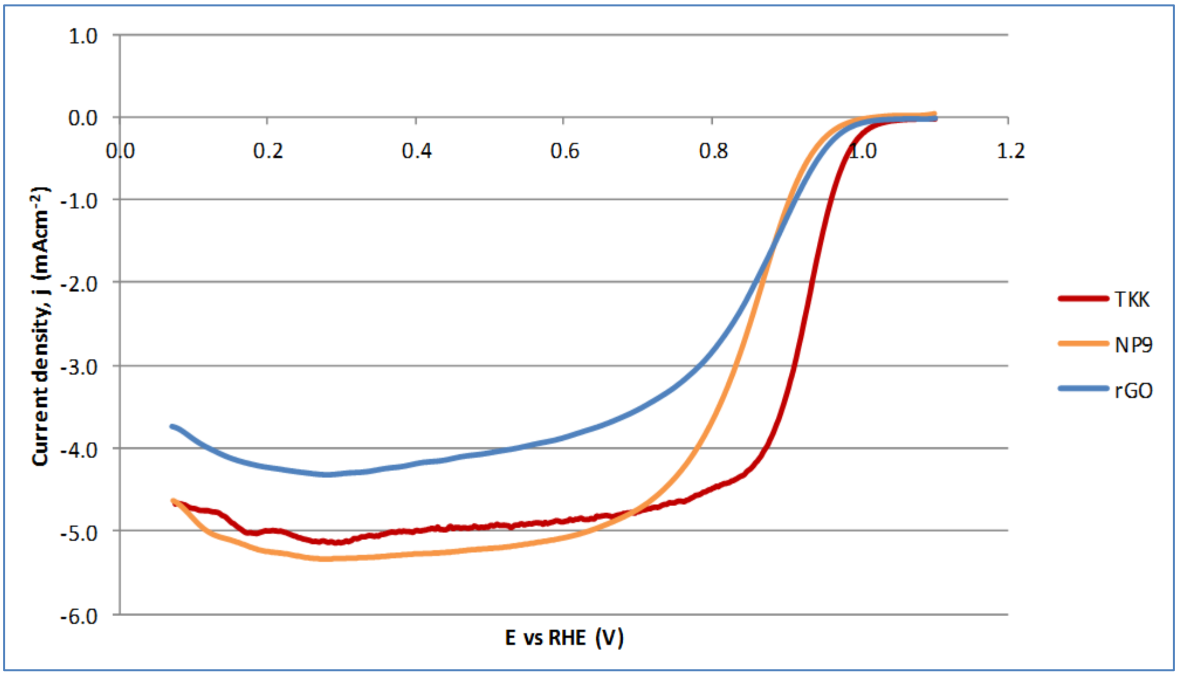

Figure 15 - Comparison of LSV scans (worst TKK/Pt/C against the best Pt/C NP-9 and Pt/GO) at 10 mV/s and 1600 rpm

Figure 15 presents the LSV curves for all three catalysts, taken at 1600 rpm. The poorest version of the TKK Pt/C was selected and still showed the lowest onset potential (when viewed as a cathodic scan) followed by the Pt/GO catalyst and the Pt/C NP-9 subsequently. This implies that the commercial TKK Pt/C has the best reactivity towards the oxygen reduction reaction.

The diffusion-limited current densities were adequately defined for the TKK Pt/C and Pt/C NP-9 catalysts and were found to be within 10% of the calculated (from the Levich equation) theoretical value of 5.7mA/cm^2 [48, 49] under the same conditions (1600 rpm, 25 °C solution temperature); this indicates an acceptable level of Pt/C film coverage on the GCE and minimal effects of oxygen diffusion in the film [48, 50]. The corresponding curve for the

Pt/GO catalyst appears have poorly formed regions of diffusion and mixed kinetics-diffusion. This suggests an inadequately set catalyst film on the GCE as well as poor oxygen diffusion in the film.

The halfwave potential, $E^{0.5}$ can also be evaluated from this plot, and is defined as the potential at the halfway point between zero current and the minimum diffusion limiting current. The E0.5 value is indicative of the catalyst activity. Table 2 summarises the obtained half wave potentials.

Catalyst	***Half wave potential, $E^{0.5}$ (V)***
TKK Pt/C	0.916
Pt/GO	0.848
Pt/C NP-9	0.844

Table 2 Half wave potentials obtained from LSV at 1600 rpm

Finally, as seen in Figure 15 a slight decrease in limiting current at potentials below 0.3 V, indicative of deviation from a four electron to a two electron reaction pathway, resulting in the formation of H_2O_2 [64].

The LSV curve for Pt/GO appears to be poorly formed. The small slope for the mixed kinetic and diffusion region indicates the possible inadequate coverage of catalyst ink on the GCE and oxygen diffusion effects characteristic of a bad ink film. Furthermore, the diffusion limited current region appears to be irregular, alluding to poor diffusion or mass transport to the Pt/GO catalyst film.

Catalyst	SA (μA/cm2)		MA (A/mg)		Reference
	0.90 V	**0.95 V**	**0.90 V**	**0.95 V**	
TKK Pt/C	467.23	87.95	0.396	0.074	This work
Pt/C NP-9	807.67	168.37	0.068	0.014	
Pt/GO	265.24	78.38	0.059	0.017	
TKK Pt/C	292	-	0.27	-	Ref. [57]

Table 3 Summary of ORR-evaluated specific area (SA) and mass (MA) activities

Table 3 shows the specific activity and mass activity evaluated at 0.9 V and 0.95 V respectively. Catalyst activity for the ORR is generally evaluated at these potentials. According to Gasteiger et al. [61], this is because the interference of mass transport losses cannot be dismissed at higher current densities observed below 0.9 V. The values obtained in this study were compared against those obtained in previous works.

It is noted that even for the TKK Pt/C catalyst, the specific and mass activities obtained from this work were much higher than that found in literature. The Pt/C NP-9 catalyst showed the highest activities towards the ORR. This finding was counter intuitive, especially since the ECSA values for the same catalyst were the lowest among the three.

The Pt/GO catalyst on the other hand showed comparable specific activity to the commercial catalyst in literature, but poorer mass activity. Perhaps this indicates good surface coverage of Pt on the graphene nanosheets but inaccessibility of the reactants to the Pt nanoparticles embedded in between the layers of graphene. The low mass activity values obtained here may be cross referenced to Figure 15, where the low slope kinetic region indicated that the Pt/GO film was inadequately formed. In this case, Garsany et al. [65] had previously reported ca. 55% difference in Pt mass activity between good films and bad films.

5.3 Catalyst Degradation

As mentioned previously, the ECSA was measured and calculated every 1200 cycles of ADT. These ECSA values were used to chart the rate of deterioration of the catalysts. The following figure presents the degradation profiles of the three catalysts.

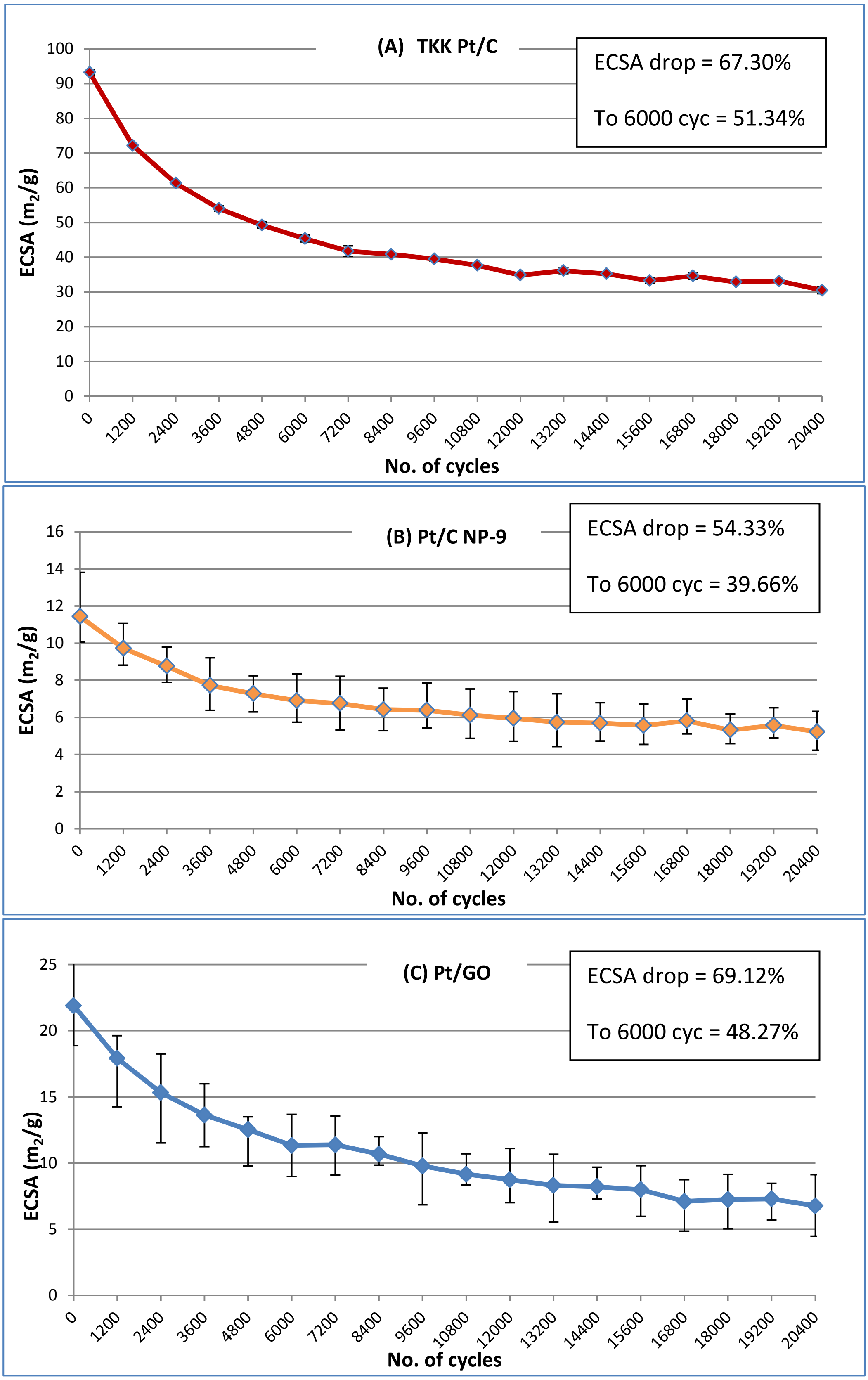

Figure 16 - Average ECSA degradation for (A) TKK Pt/C, (B) Pt/C NP-9, and (C) Pt/GO

Figure 16 shows the ECSA deterioration profiles for TKK Pt/C, Pt/C NP-9 and Pt/GO over 20400 cycles of square wave potential cycling. The catalyst films were cycled between 0.6 V (oxidised) and 1.2 V (reduced) at high speeds to simulate the typical potential load conditions of a fuel cell. The ECSA measurements were taken after every 1200 cycles in the following order: 250mV/s (conditioning) and a set of 25mV/s in linear and staircase scans each.

It is first noted that the deterioration of the ECSA does not occur in a linear manner. As such, it would be an unfair representation to calculate an average loss rate of ECSA for the catalysts. Over 20400 cycles, the ECSA deteriorates by 67.30% but after 6000 cycles 51.34% of the ECSA has already been lost. From 6000 cycles onwards, the degradation appears to stabilise. This observation was also made by Cheng et al. [60]. Again the error bars indicate the range of values obtained in repeat experiments and these appear to still be narrow, reflecting the consistency of the catalysts tested.

The deterioration of ECSA in catalyst films can be caused by degradation of the catalyst and/or support. In their review paper, Zhang et al. noted that there were three reasons for catalyst degradation: (1) Pt particle agglomeration and particle growth, (2) Pt loss and redistribution and (3) poisonous effects caused by contaminants [66]. Carbon corrosion can also lead to dislodgement of Pt nanoparticles and sever the electrical contact between the catalyst and conductor, rendering the catalyst useless.

There has not been a general agreement for an underlying mechanism of the respective contributions of the reasons mentioned above [67]. Shao et al. [68] noted that proposed degradation mechanisms in different works tended to be specific also to the conditions of the different investigations. As such, finding the most accurate mechanism of degradation requires an understanding of the working conditions. In this instance of load cycling, the dissolution/precipitation mechanism may be most appropriate [69]. As noted by Wang et al. potential cycling between Pt oxide formation (+1.2 V) and reduction (+0.6 V) results in high dissolution rates, being three to four orders of magnitude higher than potential holding in the oxide formation region. When the Pt oxides are reduced in the negative potential sweep, Pt^{Z+} ions are created and these dissolve in electrolyte [6, 7]. Accelerated corrosion was then observed in sulphuric acid systems [72]. Mitsushima et al. [71] further proposed that two types of Pt oxide were formed: the first being a thin monolayer formed during mild oxidation and the other being a thick, highly hydrated, porous, polymer like oxide with a relatively open structure, formed under severe oxidation. In a separate study, it was concluded that the number of cycles was the main contributor ECSA loss in Pt catalysts and the time spent at high potentials was a secondary factor [73]. However, the latter parameter was not tested in this study.

It was noted that lowest ECSA loss was with Pt/C NP-9 (Figure 16B). Over 20400 cycles of potential cycling, the 54.33% decrease in the ECSA from the initial value suggests a greater durability than even the commercial TKK Pt/C catalyst. In a study that employed Nafion® as the Pt nanoparticle stabiliser, it was inferred that the polymer has an adhesive and steric effect on the Pt nanoparticles thereby restricting mobility and agglomeration [60]. The adhesive effect binds the Pt clusters to the support material, and the steric effect may resist agglomeration even if migration occurs.

The Pt/GO catalyst showed the largest ECSA drop (69.12%) among the three catalysts tested. Not much can be said in certainty (without conclusive imaging evidence) about the role of graphene oxide in causing the poor durability of the catalyst. However, it is inferred that the nanosheet structure may in fact be a poor support for Pt nanoparticles, having little to no porosity. As such, all Pt nanoparticles would adhere to the surface of these nanosheets and consequently be easily dissolved, removed or agglomerated.

5.3 Correlation between Structure and Performance

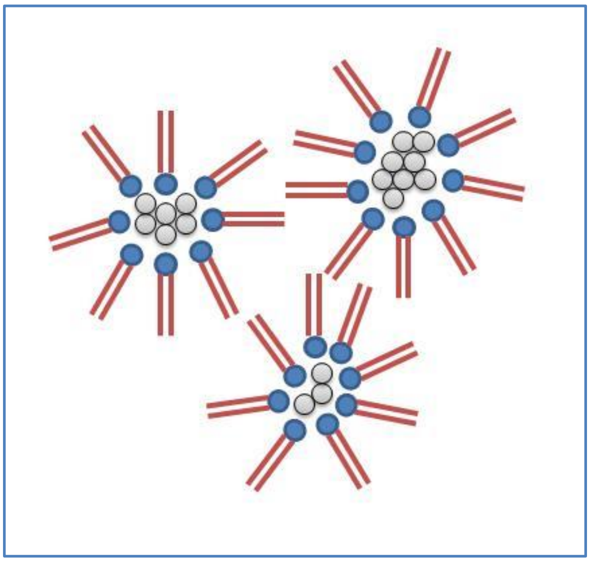

Figure 17 - Diagrammatic illustration of surfactant interactions with Pt nanoparticles

Hahakura et al. [74] proposed that in the presence of a large amount of surfactant, Pt nanoparticles can be completely ‘coated’ by surfactant molecules. This separates nanoparticle clusters from one another and thus prevents aggregation. However, there are drawbacks to having surfactant coverage as the active sites may be blocked and the performance of the catalyst consequently impaired. Some works have therefore looked into a treatment method to remove the surfactant once the Pt nanoparticles have been reduced on its corresponding support material. It has also been shown that the electrochemically active area increases if the catalysts are washed with ethanol [29]. However, it is important to note that rinsing with organic solvents tends to leave traces/films on Pt surfaces that may alter electrochemical kinetics. Hui et al. [29] reported that the hydrogen adsorption/desorption peaks for catalysts increased in the order of untreated < centrifugation < ethanol wash.

Previous research has also seen the Pt oxide reduction peak shift towards the negative when the ratio of surfactant to Pt was increased, possibly due to the size effects of Pt nanoparticles on oxide reduction potentials [74, 75]. This feature was suspected for the Pt/C NP-9 CV in Figure 14, but not definitive.

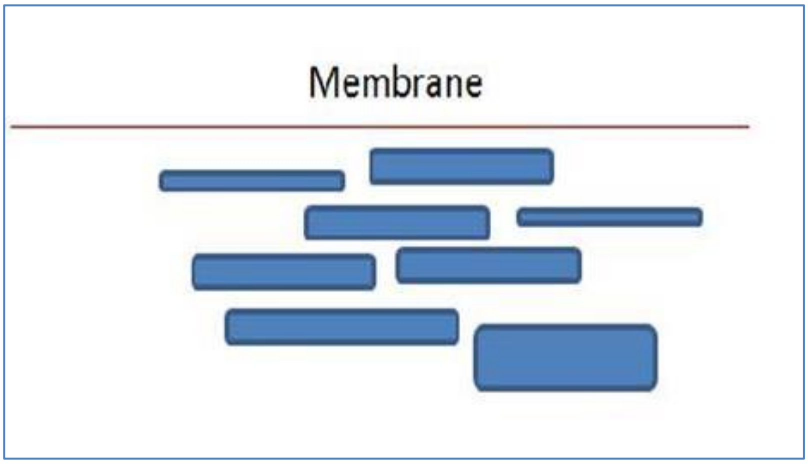

Figure 18 - Diagrammatic illustration of general GO orientation in the catalyst film

As graphene nanosheets tend to be stacked horizontally, there is a high probability of a large amount of Pt active sites being locked in between the layers; these Pt catalysts would be wastefully inaccessible and therefore not contribute to the ECSA. This phenomena was also hypothesised by Park et al.[37], who subsequently showed that the addition of carbon black to Pt/graphene catalysts increased Pt utilisation by exposing the Pt nanoparticles that were trapped between superimposed graphene sheets. Other than that, the presence of thick unexfoliated graphite flakes could result in poor Pt catalyst nanoparticle dispersion besides having a high capacitance [77], as evidenced by the thick capacitance region seen in Figure 28 (Appendix 8.2.3). Both are plausible contributors to the poor performance observed.

Different preparation routes may also improve the desirable properties of graphene supports. For instance, Lei et al. [43] showed that polydiallyldimethylammonium improve Pt distribution on graphene supports, consequently improving the ECSA and catalyst activities. More precise centrifugation could also be used to isolate the layered graphene oxide from the thicker unexfoliated graphite flakes. It was also shown that graphene doped on carbon black supports showed high durability and high mass activity due to a highly uniformed distribution of Pt nanoparticles on the surface of the support [78].

5.4 Other Observations

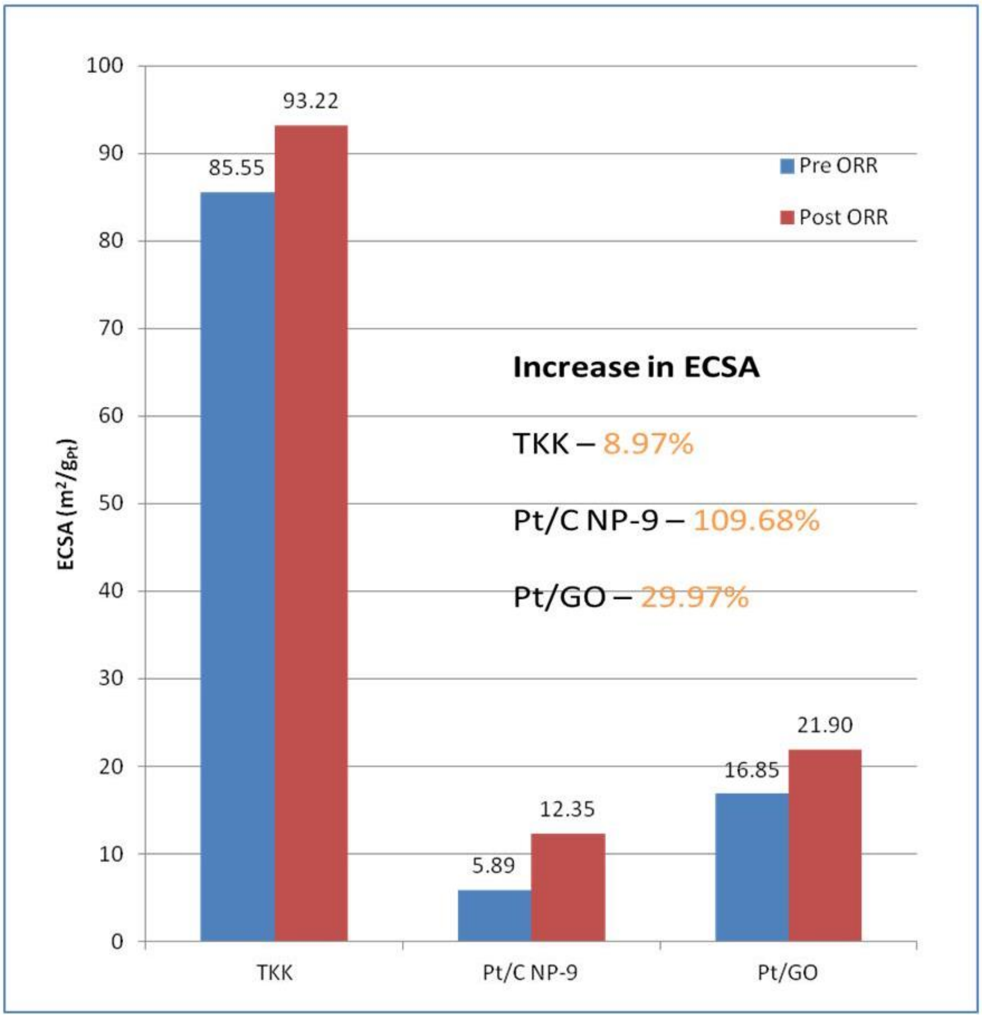

Figure 19 - Pre- vs Post-ORR ECSA values

An interesting observation was made when comparing ECSA values before and after LSV scans. Catalyst films were initially conditioned (high speed CVs repeated 100 to 150 times) until no significant changes in CV profiles were observed; after which CV tests were performed at different scan rates and their corresponding ECSA values obtained. However, improvements in ECSA values were seen after ORR testing (repeated LSV and CV conditioning cycles at different rotation speeds).

It is noted from the figure above that the catalysts containing the NP-9 surfactant had a two-fold increase in ECSA value after the ORR testing procedure. As this procedure involved repeated potential cycling and oxygenation of the solution, it is possible that the catalysts underwent several conditioning cycles. Alternatively, the peroxide produced by the ORR could have acted as a washing agent, stripping the NP-9 surfactant from the Pt nanoparticles thus uncovering more active sites. The commercial TKK Pt/C catalyst showed the lowest change in ECSA followed by the Pt/GO catalyst, alluding to the difference in stability of both catalysts. It is possible that the Pt/C NP-9 catalyst did not undergo physical changes from potential cycling; rather, the repeated potential cycling may have mobilised the surfactant molecules away from Pt cluster, thus exposing active sites that may have been shielded by the surfactant. Figure 26 in the appendix shows a much larger Pt oxidation and Pt oxide reduction region after ORR tests, supporting the suggestion that peroxide may have ‘washed’ off excess surfactant molecules from Pt surfaces.

6.0 Conclusions & Recommendations

6.1 Conclusions

It is noted that the benchmark catalyst (TKK TEC10E50E 45.9 wt. %) outperforms the novel surfactant (NP-9) doped catalyst and reduced graphene oxide (rGO) supported catalyst quite significantly. While the TKK catalyst achieved ECSA values in excess of 80 m^2/g_{Pt}, the NP-9 doped catalyst and rGO supported catalyst generally achieved ECSAs below 40 m^2/g_{Pt}.

Between the two, it was observed that the NP-9 doped catalyst showed the lowest range of ECSA values. This could be attributed to steric interference that prevents the Pt nanoparticles from adhering to the support material, leading to poor electrical contact, catalyst dislodgement and movement. However, the shielding provided by surfactant molecules on Pt nanoparticles appears to obstruct, or at least limit aggregation; this was evident in the ADT results where the Pt/C NP-9 catalyst showed the lowest loss of ECSA over 20400 cycles. The encapsulation of the Pt active sites by the surfactant molecules also appears to be reversible, or dynamic in some sense, indicated by the increase in ECSA values post-ORR testing. On the other hand, it is more likely that the peroxide product from the ORR tests reacted with the surfactant and thus uncovered Pt sites that were previously shielded.

Surfactant encapsulation of Pt active sites appears to have enhanced the catalyst activity towards the ORR and also its durability. Values for mass and specific activity were almost double that of the commercial catalyst and when compared to the other two catalysts used in this study (including the benchmark TKK catalyst), the Pt/C NP-9 catalyst also showed the lowest ECSA decrease with voltage cycling in excess of 20000 cycles. This implies that the surfactant does in fact hinder Pt nanoparticle aggregation and dissolution quite effectively. Since catalyst durability is an essential criterion for the commercialisation of PEMFCs, the surfactant route may hold the key towards improving catalyst durability to make it more competitive with current technologies.

The rGO supported catalyst showed the most mediocre performance among the three, with no distinctly unique results. It is likely that the sheet structure of graphene impedes the mass transfer of reactants to and from the catalyst active sites by forcing a longer pathway. Although it showed higher ECSA values than the Pt/C NP-9 catalyst initially (possibly owing to the high electrical conductivity of rGO), poor ORR performance and durability are good reasons to dismiss Pt/GO as a good catalyst for PEFC based on the conditions and evidence in this study.

6.2 Recommendations

It is widely understood that *ex-situ* characterisation of PEMFC catalysts seldom reflect the true performance of the catalysts in real-world applications (consolidation of ex-situ and in-situ methods would constitute a major step forward in evaluating PEMFC catalysts). *Ex-situ* characterisation merely serves as a screen for inferior and non-functional catalysts. As such, in situ characterisation i.e. application of catalyst inks onto a PEMFC membrane electrode assembly (MEA) is necessary to gauge the actual performance of the novel catalyst inks. Naturally this step introduces various new parameters such as humidity, gas flow, plate compression etc. However, until more accurate representative *ex-situ* methods are developed, this step is vital towards the successful introduction and commercialisation of all novel PEMFC catalysts.

A greater understanding of surfactant interactions with Pt could prove pivotal in improving the durability of novel catalysts. Being able to manipulate the Pt-surfactant interactions could also capitalise on the shielding effect, resulting in smaller average sizes of Pt nanoparticles which maximises the electrochemical surface area.

Recent PEMFC studies related to graphene have shown some inclination towards manipulating graphene through nitrogen doping or combining graphene with high surface area carbon supports to improve the electron conductivity of the material [41, 61]. This method is likely to yield positive results and should also be further investigated. Alternatively, reducing the average size of the graphene sheets may reduce the mass transport resistance and therefor optimise the performance of the catalysts.

7.0 References

[1] A. Fensom, “Japan: On the Cusp of Energy Independence?,” *The Diplomat*, 2013. [Online]. Available: http://thediplomat.com/pacific-money/2013/03/26/japan-on-the-cusp-of-energy-independence/.

[2] P. F. Troy, “Oil shale discovery in South Australis proves significant,” *PennEnergy*, 2011. [Online]. Available: http://www.pennenergy.com/index/blogs/all-energy-all-the-time/2011/09/oil-shale-discovery-in-south-australia-proves-significant.html. [Accessed: 24-Apr-2013].

[3] B. Lefebvre, “Critics Warn of Environmental Hazards IN Extracting Methane Hydrate,” *The Wall Street Journal*, 2013. [Online]. Available: http://online.wsj.com/article/SB10001424127887323664204578610370550437906.html. [Accessed: 10-Aug-2013].

[4] R. Webster, “Does the financial sector believe in unburnable carbon?,” *The Carbon Brief*, 2013. [Online]. Available: http://www.carbonbrief.org/blog/2013/02/will-the-financial-community-respond-carbon-bubble. [Accessed: 31-Mar-2013].

[5] “Svante Arrhenius (1859-1927),” *NASA Earth Observatory*. [Online]. Available: http://earthobservatory.nasa.gov/Features/Arrhenius/arrhenius.php. [Accessed: 20-Jan-2013].

[6] S. Evans, “Germany: Nuclear power platns to close by 2022,” *BBC*, 2011. [Online]. Available: http://www.bbc.co.uk/news/world-europe-13592208. [Accessed: 12-Jan-2013].

[7] M. Shuttleworth, “Heron’s Inventions,” *Explorable.com*, 2011. [Online]. Available: http://explorable.com/heron-inventions. [Accessed: 28-Nov-2012].

[8] U. Bossel and B. Eliasson, “Energy and the Hydrogen Economy,” 2003.

[9] R. Masel and G. Mozsgai, “Liquid feed fuel cell with nested sealing configuration,” US73723267 B22008.

[10] E. I. Centre, “Comparison of Fuel Cell Technologies,” 2011. [Online]. Available: http://www1.eere.energy.gov/hydrogenandfuelcells/fuelcells/pdfs/fc_comparison_chart.pdf.

[11] G. Zhang, S. Sun, M. Cai, Y. Zhang, R. Li, and X. Sun, “Porous dendritic platinum nanotubes with extremely high activity and stability for oxygen reduction reaction.,” *Sci. Rep.*, vol. 3, p. 1526, Jan. 2013.

[12] C. Kim, J.-G. Oh, Y.-T. Kim, H. Kim, and H. Lee, “Platinum dendrites with controlled sizes for oxygen reduction reaction,” *Electrochem. commun.*, vol. 12, no. 11, pp. 1596–1599, Nov. 2010.

[13] X. Yao, K. Su, S. Sui, L. Mao, A. He, J. Zhang, and S. Du, “A novel catalyst layer with carbon matrix for Pt nanowire growth in proton exchange membrane fuel cells (PEMFCs),” *Int. J. Hydrogen Energy*, vol. 8, pp. 2–6, Aug. 2013.

[14] Y.-J. Hsueh, C.-C. Yu, K.-R. Lee, C.-J. Tseng, B.-J. Su, S.-K. Wu, and L.-C. Weng, “Ordered porous carbon as the catalyst support for proton-exchange membrane fuel cells,” *Int. J. Hydrogen Energy*, vol. 38, no. 25, pp. 10998–11003, Aug. 2013.

[15] Y. Zhang, C. Ma, Y. Zhu, R. Si, Y. Cai, J. X. Wang, and R. R. Adzic, “Hollow core supported Pt monolayer catalysts for oxygen reduction,” *Catal. Today*, vol. 202, pp. 50–54, Mar. 2013.

[16] J. D. A. Iii and R. G. Finke, “A review of modern transition-metal nanoclusters : their synthesis , characterization , and applications in catalysis,” 1999.

[17] B. C. Rostro-Kohanloo, L. R. Bickford, C. M. Payne, E. S. Day, L. J. E. Anderson, M. Zhong, S. Lee, K. M. Mayer, T. Zal, L. Adam, C. P. N. Dinney, R. a Drezek, J. L. West, and J. H. Hafner, “The stabilization and targeting of surfactant-synthesized gold nanorods.,” *Nanotechnology*, vol. 20, no. 43, p. 434005, Oct. 2009.

[18] S. De, A. Pal, N. R. Jana, and T. Pal, “Anion effect in linear silver nanoparticle aggregation as evidenced by efficient fluorescence quenching and SERS enhancement,” *J. Photochem. Photobiol. A Chem.*, vol. 131, no. 1–3, pp. 111–123, Feb. 2000.

[19] B. A. Larsen, M. A. Haag, N. J. Serkova, K. R. Shroyer, and C. R. Stoldt, “Controlled aggregation of superparamagnetic iron oxide nanoparticles for the development of molecular magnetic resonance imaging probes.,” *Nanotechnology*, vol. 19, no. 26, p. 265102, Jul. 2008.

[20] A. Graf, E. Ablinger, S. Peters, A. Zimmer, S. Hook, and T. Rades, “Microemulsions containing lecithin and sugar-based surfactants: nanoparticle templates for delivery of proteins and peptides.,” *Int. J. Pharm.*, vol. 350, no. 1–2, pp. 351–60, Mar. 2008.

[21] J. Xie, D. L. Wood, K. L. More, P. Atanassov, and R. L. Borup, “Microstructural Changes of Membrane Electrode Assemblies during PEFC Durability Testing at High Humidity Conditions,” *J. Electrochem. Soc.*, vol. 152, no. 5, p. A1011, May 2005.

[22] E. Guilminot, A. Corcella, F. Charlot, F. Maillard, and M. Chatenet, “Detection of Pt[sup z+] Ions and Pt Nanoparticles Inside the Membrane of a Used PEMFC,” *J. Electrochem. Soc.*, vol. 154, no. 1, p. B96, 2007.

[23] G. X. Wang, L. Yang, J. Z. Wang, H. K. Liu, and S. X. Dou, "Enhancement of ionic conductivity of PEO based polymer electrolyte by the addition of nanosize ceramic powders.," *J. Nanosci. Nanotechnol.*, vol. 5, no. 7, pp. 1135–40, Jul. 2005.

[24] T. Yonezawa, Y. Gotoh, and N. Toshima, "Protecting structure model for nanoscopic platinum clusters protected by non-ionic surfactants: 13C nuclear magnetic resonance investigation," *React. Polym.*, vol. 23, no. 2–3, pp. 43–51, Oct. 1994.

[25] J. Tanori, N. Duxin, C. Petit, I. Lisiecki, P. Veillet, and M. P. Pileni, "Synthesis of nanosize metallic and alloyed particles in ordered phases," *Colloid Polym. Sci.*, vol. 273, no. 9, pp. 886–892, Sep. 1995.

[26] X. Wang and I.-M. Hsing, "Surfactant stabilized Pt and Pt alloy electrocatalyst for polymer electrolyte fuel cells," *Electrochim. Acta*, vol. 47, no. 18, pp. 2981–2987, Jul. 2002.

[27] H. Bonnemann, G. Braun, W. Brijoux, R. Brinkmann, A. S. Tilling, K. Seevogel, and K. Siepen, "Nanoscale colloidal metals and alloys stabilized by solvents and surfactants Preparation and use as catalyst precursors," *J. Organomet. Chem.*, vol. 520, pp. 143–162, 1996.

[28] D.-H. Lim, W.-D. Lee, D.-H. Choi, D.-R. Park, and H.-I. Lee, "Preparation of platinum nanoparticles on carbon black with mixed binary surfactants: Characterization and evaluation as anode catalyst for low-temperature fuel cell," *J. Power Sources*, vol. 185, no. 1, pp. 159–165, Oct. 2008.

[29] C. L. Hui, X. G. Li, and I.-M. Hsing, "Well-dispersed surfactant-stabilized Pt/C nanocatalysts for fuel cell application: Dispersion control and surfactant removal," *Electrochim. Acta*, vol. 51, no. 4, pp. 711–719, Nov. 2005.

[30] S. Chen and K. Kimura, "Synthesis and Characterization of Carboxylate-Modified Gold Nanoparticle Powders Dispersible in Water," *Langmuir*, vol. 15, no. 4, pp. 1075–1082, Feb. 1999.

[31] S.-G. Hong, E. S. Lee, J.-Y. Bae, M.-J. Lee, H. Chang, and D. Y. Seung, "Effects of amphiphilic surfactants on electrolyte distribution in polymer electrolyte fuel-cell electrode," *J. Mater. Res.*, vol. 22, no. 12, pp. 3355–3359, Jan. 2011.

[32] R. G. A. G. a. Wills, M. J. Watt-Smith, and F. C. C. Walsh, "The Use of Fluorocarbon Surfactants to Improve the Manufacture of PEM Fuel Cell Electrodes," *Fuel Cells*, vol. 9, no. 2, pp. 148–156, Apr. 2009.

[33] B. Seger and P. V. Kamat, "Electrocatalytically Active Graphene-Platinum Nanocomposites. Role of 2-D Carbon Support in PEM Fuel Cells," *J. Phys. Chem. C*, vol. 113, no. 19, pp. 7990–7995, May 2009.

[34] L. Yun-Xia, Z.-D. WEI, Z. Qian-Ling, D. Wei, Z. Qian, and C. Si-Guo, "Preparation of Pt / Graphene Catalyst and Its Catalytic Performance for Oxygen Reduction," *Acta Phisico-Chimica Sin.*, vol. 27, no. 4, pp. 858–862, 2011.

[35] H.-W. Ha, I. Y. Kim, S.-J. Hwang, and R. S. Ruoff, "One-Pot Synthesis of Platinum Nanoparticles Embedded on Reduced Graphene Oxide for Oxygen Reduction in Methanol Fuel Cells," *Electrochem. Solid-State Lett.*, vol. 14, no. 7, p. B70, 2011.

[36] J. H. Jung, H. J. Park, J. Kim, and S. H. Hur, "Highly durable Pt/graphene oxide and Pt/C hybrid catalyst for polymer electrolyte membrane fuel cell," *J. Power Sources*, vol. 248, pp. 1156–1162, Feb. 2014.

[37] S. Park, Y. Shao, H. Wan, P. C. Rieke, V. V. Viswanathan, S. a. Towne, L. V. Saraf, J. Liu, Y. Lin, and Y. Wang, "Design of graphene sheets-supported Pt catalyst layer in PEM fuel cells," *Electrochem. commun.*, vol. 13, no. 3, pp. 258–261, Mar. 2011.

[38] X. Liu, J. Duan, H. Chen, Y. Zhang, and X. Zhang, "A carbon riveted Pt/Graphene catalyst with high stability for direct methanol fuel cell," *Microelectron. Eng.*, vol. 110, pp. 354–357, Oct. 2013.

[39] M. N. Groves, a. S. W. Chan, C. Malardier-Jugroot, and M. Jugroot, "Improving platinum catalyst binding energy to graphene through nitrogen doping," *Chem. Phys. Lett.*, vol. 481, no. 4–6, pp. 214–219, Oct. 2009.

[40] D. He, Y. Jiang, H. Lv, M. Pan, and S. Mu, "Nitrogen-doped reduced graphene oxide supports for noble metal catalysts with greatly enhanced activity and stability," *Appl. Catal. B Environ.*, vol. 132–133, pp. 379–388, Mar. 2013.

[41] T. Hibino, K. Kobayashi, and P. Heo, "Oxygen reduction reaction over nitrogen-doped graphene oxide cathodes in acid and alkaline fuel cells at intermediate temperatures," *Electrochim. Acta*, vol. 112, pp. 82–89, Dec. 2013.

[42] Y. Xin, J. Liu, X. Jie, W. Liu, F. Liu, Y. Yin, J. Gu, and Z. Zou, "Preparation and electrochemical characterization of nitrogen doped graphene by microwave as supporting materials for fuel cell catalysts," *Electrochim. Acta*, vol. 60, pp. 354–358, Jan. 2012.

[43] M. Lei, C. Liang, Y. J. Wang, K. Huang, C. X. Ye, G. Liu, W. J. Wang, S. F. Jin, R. Zhang, D. Y. Fan, H. J. Yang, and Y. G. Wang, "Durable platinum/graphene catalysts assisted with polydiallyldimethylammonium for proton-exchange membrane fuel cells," *Electrochim. Acta*, vol. 113, pp. 366–372, Dec. 2013.

[44] B. Xiong, Y. Zhou, Y. Zhao, J. Wang, X. Chen, R. O'Hayre, and Z. Shao, "The use of nitrogen-doped graphene supporting Pt nanoparticles as a catalyst for methanol electrocatalytic oxidation," *Carbon N. Y.*, Sep. 2012.

[45] Z. Lin, G. H. Waller, Y. Liu, M. Liu, and C. Wong, "Simple preparation of nanoporous few-layer nitrogen-doped graphene for use as an efficient electrocatalyst for oxygen

reduction and oxygen evolution reactions," *Carbon N. Y.*, vol. 53, pp. 130–136, Mar. 2013.

[46] B. Zheng, J. Wang, F.-B. Wang, and X.-H. Xia, "Synthesis of nitrogen doped graphene with high electrocatalytic activity toward Oxygen Reduction Reaction," *Electrochem. commun.*, vol. 28, pp. 24–26, Dec. 2012.

[47] a. Menzel, K. Swamy, R. Beer, P. Hanesch, E. Bertel, and U. Birkenheuer, "Electronic structure of a catalyst poison: Br/Pt(110)," *Surf. Sci.*, vol. 454–456, pp. 88–93, May 2000.

[48] M. Goor-Dar, N. Travitsky, and E. Peled, "Study of hydrogen redox reactions on platinum nanoparticles in concentrated HBr solutions," *J. Power Sources*, vol. 197, pp. 111–115, Jan. 2012.

[49] A. K. Geim and K. S. Novoselov, "The rise of graphene.," *Nat. Mater.*, vol. 6, no. 3, pp. 183–91, Mar. 2007.

[50] D. a. C. Brownson, D. K. Kampouris, and C. E. Banks, "An overview of graphene in energy production and storage applications," *J. Power Sources*, vol. 196, no. 11, pp. 4873–4885, Jun. 2011.

[51] V. Singh, D. Joung, L. Zhai, S. Das, S. I. Khondaker, and S. Seal, "Graphene based materials: Past, present and future," *Prog. Mater. Sci.*, vol. 56, no. 8, pp. 1178–1271, Oct. 2011.

[52] E. Antolini, "Graphene as a new carbon support for low-temperature fuel cell catalysts," *Appl. Catal. B Environ.*, vol. 123–124, pp. 52–68, Jul. 2012.

[53] C.-T. Hsieh, J.-M. Wei, J.-S. Lin, and W.-Y. Chen, "Pulse electrodeposition of Pt nanocatalysts on graphene-based electrodes for proton exchange membrane fuel cells," *Catal. Commun.*, vol. 16, no. 1, pp. 220–224, Nov. 2011.

[54] E. Yoo, T. Okada, T. Akita, M. Kohyama, I. Honma, and J. Nakamura, "Sub-nano-Pt cluster supported on graphene nanosheets for CO tolerant catalysts in polymer electrolyte fuel cells," *J. Power Sources*, vol. 196, no. 1, pp. 110–115, Jan. 2011.

[55] E. Yoo, T. Okata, T. Akita, and M. Kohyama, "Enhanced Electrocatalytic Activity of Pt Subnanoclusters on Graphene 2009," vol. 2, no. 2, pp. 4–8, 2009.

[56] Y. Garsany, I. L. Singer, and K. E. Swider-Lyons, "Impact of film drying procedures on RDE characterization of Pt/VC electrocatalysts," *J. Electroanal. Chem.*, vol. 662, no. 2, pp. 396–406, Nov. 2011.

[57] I. Takahashi and S. S. Kocha, "Examination of the activity and durability of PEMFC catalysts in liquid electrolytes," *J. Power Sources*, vol. 195, no. 19, pp. 6312–6322, Oct. 2010.

[58] M. K. Debe, “Electrocatalyst approaches and challenges for automotive fuel cells.,” *Nature*, vol. 486, no. 7401, pp. 43–51, Jun. 2012.

[59] EG&G Technical Services, *Fuel cell handbook*, 7th ed., no. November. West Virginia: US Department of Energy, Office of Fossil Energy, 2004.

[60] N. Cheng, S. Mu, M. Pan, and P. P. Edwards, “Improved lifetime of PEM fuel cell catalysts through polymer stabilization,” *Electrochem. commun.*, vol. 11, no. 8, pp. 1610–1614, Aug. 2009.

[61] H. A. Gasteiger, S. S. Kocha, B. Sompalli, and F. T. Wagner, “Activity benchmarks and requirements for Pt , Pt-alloy , and non-Pt oxygen reduction catalysts for PEMFCs,” vol. 56, pp. 9–35, 2005.

[62] K. J. J. Mayrhofer, D. Strmcnik, B. B. Blizanac, V. Stamenkovic, M. Arenz, and N. M. Markovic, “Measurement of oxygen reduction activities via the rotating disc electrode method: From Pt model surfaces to carbon-supported high surface area catalysts,” *Electrochim. Acta*, vol. 53, no. 7, pp. 3181–3188, Feb. 2008.

[63] U. a. Paulus, T. J. Schmidt, H. a. Gasteiger, and R. J. Behm, “Oxygen reduction on a high-surface area Pt/Vulcan carbon catalyst: a thin-film rotating ring-disk electrode study,” *J. Electroanal. Chem.*, vol. 495, no. 2, pp. 134–145, Jan. 2001.

[64] N. M. Markovic and P. N. Ross Jr, “Surface science studies of model fuel cell electrocatalysts,” *Surf. Sci. Rep.*, vol. 45, pp. 117–229, 2002.

[65] Y. Garsany, O. a Baturina, K. E. Swider-Lyons, and S. S. Kocha, “Experimental methods for quantifying the activity of platinum electrocatalysts for the oxygen reduction reaction.,” *Anal. Chem.*, vol. 82, no. 15, pp. 6321–8, Aug. 2010.

[66] S. Zhang, X. Yuan, J. Ng, C. Hin, H. Wang, K. A. Friedrich, and M. Schulze, “A review of platinum-based catalyst layer degradation in proton exchange membrane fuel cells,” vol. 194, pp. 588–600, 2009.

[67] P. J. Ferreira, G. J. la O’, Y. Shao-Horn, D. Morgan, R. Makharia, S. Kocha, and H. A. Gasteiger, “Instability of Pt⁄C Electrocatalysts in Proton Exchange Membrane Fuel Cells,” *J. Electrochem. Soc.*, vol. 152, no. 11, p. A2256, Nov. 2005.

[68] Y. Shao, G. Yin, and Y. Gao, “Understanding and approaches for the durability issues of Pt-based catalysts for PEM fuel cell,” *J. Power Sources*, vol. 171, no. 2, pp. 558–566, Sep. 2007.

[69] C. He, S. Desai, G. Brown, and S. Bollepalli, “PEM Fuel Cell Catalysts: Cost, Performance, and Durability,” *Interface*, vol. 14, pp. 41–44, 2005.

[70] Z. Nagy and H. You, “Applications of surface X-ray scattering to electrochemistry problems,” *Electrochim. Acta*, vol. 47, no. 19, pp. 3037–3055, Jul. 2002.

[71] S. Mitsushima, S. Kawahara, K. Ota, and N. Kamiya, “Consumption Rate of Pt under Potential Cycling,” *J. Electrochem. Soc.*, vol. 154, no. 2, p. B153, Feb. 2007.

[72] K.-I. Ota, S. Nishigori, and N. Kamiya, “Dissolution of platinum anodes in sulfuric acid solution,” *J. Electroanal. Chem. Interfacial Electrochem.*, vol. 257, no. 1–2, pp. 205–215, Dec. 1988.

[73] R. L. Borup, J. R. Davey, F. H. Garzon, D. L. Wood, and M. a. Inbody, “PEM fuel cell electrocatalyst durability measurements,” *J. Power Sources*, vol. 163, no. 1, pp. 76–81, Dec. 2006.

[74] S. Hahakura, S. Isoda, T. Ogawa, S. Moriguchi, and T. Kobayashi, “Formation of ultrafine platinum particles in an aqueous solution with a surfactant,” *J. Cryst. Growth*, vol. 237–239, pp. 1942–1945, Apr. 2002.

[75] J. Prabhuram, X. Wang, C. L. Hui, and I.-M. Hsing, “Synthesis and Characterization of Surfactant-Stabilized Pt/C Nanocatalysts for Fuel Cell Applications,” *J. Phys. Chem. B*, vol. 107, no. 40, pp. 11057–11064, Oct. 2003.

[76] T. Frelink, W. Visscher, and J. a. R. van Veen, “Particle size effect of carbon-supported platinum catalysts for the electrooxidation of methanol,” *J. Electroanal. Chem.*, vol. 382, no. 1–2, pp. 65–72, Feb. 1995.

[77] J. Liu, M. Notarianni, G. Will, V. T. Tiong, H. Wang, and N. Motta, “Electrochemically exfoliated graphene for electrode films: effect of graphene flake thickness on the sheet resistance and capacitive properties.,” *Langmuir*, vol. 29, no. 43, pp. 13307–14, Oct. 2013.

[78] H. Yano, T. Akiyama, M. Watanabe, and H. Uchida, “High durability of Pt/graphitized carbon catalysts for polymer electrolyte fuel cells prepared by the nanocapsule method,” *J. Electroanal. Chem.*, Oct. 2012.

8.0 Appendices

8.1 Appendix 1 – Data Tables

8.1.1 TKK Pt/C

Scan rate (mV/s)	Area (C)	ECSA (µg/cm^2)	ECSA (m^2/g)
250	5.55E+02	0.675	67.468
100	6.21E+02	0.755	75.494
80	6.33E+02	0.769	76.895
60	6.49E+02	0.789	78.851
40	6.78E+02	0.823	82.341
20	6.97E+02	0.847	84.686
10	6.72E+02	0.817	81.661

Table 4 ECSA values obtained from linear CV for TKK Pt/C (pre-ORR)

Scan rate (mV/s)	Area (C)	ECSA (µg/cm^2)	ECSA (m^2/g)
250	6.28E+02	0.763	76.276
20	7.61E+02	0.924	92.440

Table 5 ECSA values obtained from linear CV for TKK Pt/C (post-ORR)

No of cycles	ECSA (m^2/g)
0	93.22
1200	72.19
2400	61.35
3600	54.04
4800	49.26
6000	45.36
7200	41.76
8400	40.84
9600	39.50
10800	37.69
12000	34.89
13200	36.16
14400	35.24
15600	33.28
16800	34.65
18000	32.89
19200	33.16
20400	30.48

Table 6 ECSA values after cycles of ADT for TKK Pt/C

8.1.2 Pt/C NP-9

Scan rate (mV/s)	Area (C)	ECSA (µg/cm^2)	ECSA (m^2/g)
250	3.26E+01	0.040	3.961
100	5.10E+01	0.062	6.190
80	5.56E+01	0.068	6.752
60	5.50E+01	0.067	6.677
40	6.04E+01	0.073	7.335
20	6.91E+01	0.084	8.390
10	7.11E+01	0.086	8.636

Table 7 ECSA values obtained from linear CV for Pt/C NP-9 (pre-ORR)

Scan rate (mV/s)	Area (C)	ECSA ($\mu g/cm^2$)	ECSA (m^2/g)
250	1.29E+02	0.156	15.634
20	1.24E+02	0.151	15.079

Table 8 ECSA values obtained from linear CV for Pt/C NP-9 (post ORR)

No of cycles	ECSA (m^2/g)
0	11.44
1200	9.72
2400	8.76
3600	7.72
4800	7.28
6000	6.90
7200	6.76
8400	6.41
9600	6.38
10800	6.12
12000	5.95
13200	5.74
14400	5.69
15600	5.56
16800	5.82
18000	5.31
19200	5.57
20400	5.22

Table 9 ECSA values after cycles of ADT for commercial Pt/C NP-9

8.1.3 Pt/GO

Scan rate	Area	ECSA ($\mu g/cm^2$)	ECSA (m^2/g)
250	1.66E+02	0.201	20.148
100	1.77E+02	0.215	21.538
80	1.78E+02	0.216	21.611
60	1.90E+02	0.230	23.044
40	1.75E+02	0.212	21.246
20	1.82E+02	0.221	22.101
10	1.57E+02	0.190	19.031

Table 10 ECSA values obtained from linear CV for Pt/GO (pre-ORR)

Scan rate	Area	ECSA ($\mu g/cm^2$)	ECSA (m^2/g)
250	1.75E+02	0.213	21.263
20	1.93E+02	0.234	23.413

Table 11 ECSA values obtained from linear CV for Pt/GO (post-ORR)

No of cycles	ECSA (m2/g)
0	21.90
1200	17.92
2400	15.32
3600	13.63
4800	12.53
6000	11.33
7200	11.38
8400	10.68
9600	9.78
10800	9.16
12000	8.73
13200	8.31
14400	8.20
15600	7.99
16800	7.10
18000	7.24
19200	7.29
20400	6.76

Table 12 ECSA values after cycles of ADT for commercial Pt/GO

8.1.4 Catalyst Activity

Catalyst	Pt loading (mg/cm^2)	ECSA (m^2/g)	T (°C)	Scan rate (mV/s)	SA (µA/cm2)		MA (A/mg)	
					0.90 V	0.95 V	0.90 V	0.95 V
TKK Pt/C	0.02	84.686	25	20	467.23	87.95	0.396	0.074
Pt/C NP-9	0.02	8.39	25	20	807.67	168.37	0.068	0.014
Pt/GO	0.02	22.101	25	20	265.24	78.38	0.059	0.017

Table 13 ORR-evaluated catalyst specific area (SA) and mass (MA) activities

8.2 Appendix 2 – Graphs

8.2.1 TKK Pt/C

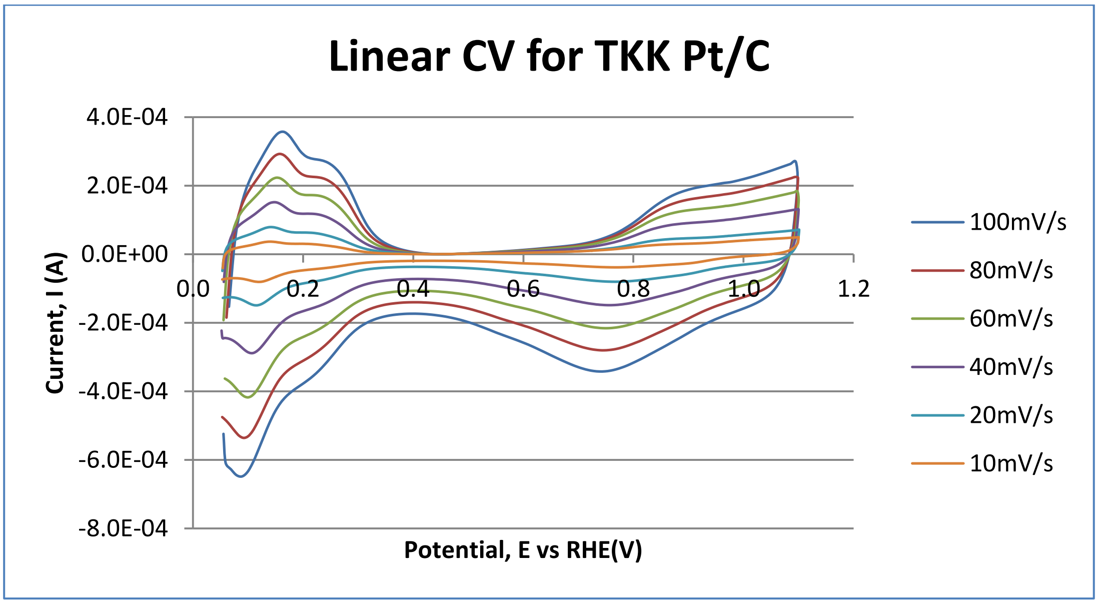

Figure 20 - Linear CV for TKK Pt/C in 0.1 m $HClO_4$

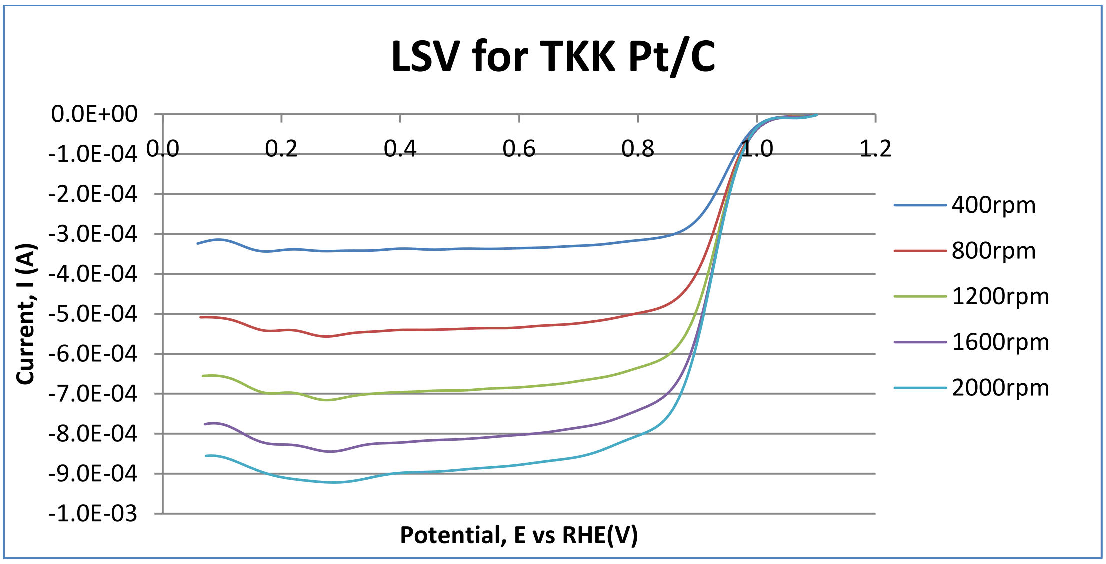

Figure 21 - LSV for TKK Pt/C in oxygen saturated 0.1 M $HClO_4$

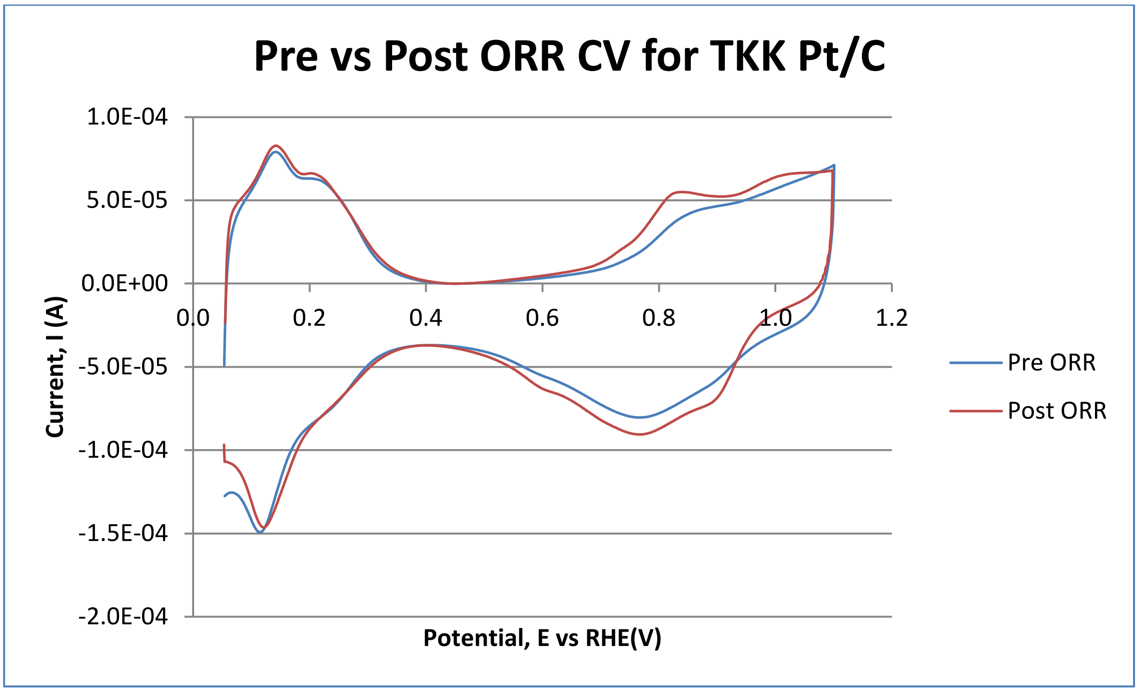

Figure 22 - Pre- vs Post-ORR Linear CV for TKK Pt/C in 0.1 M $HClO_4$

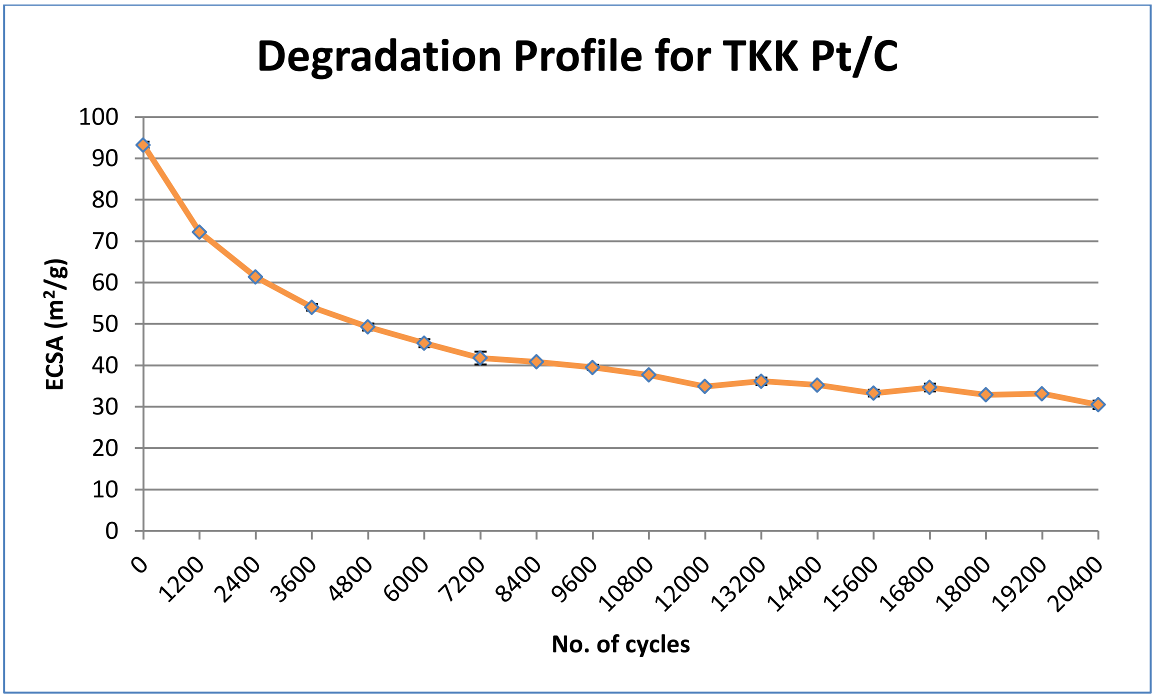

Figure 23 - ADT ECSA profile for TKK Pt/C in 0.1 M $HClO_4$

8.2.2 Pt/C NP-9

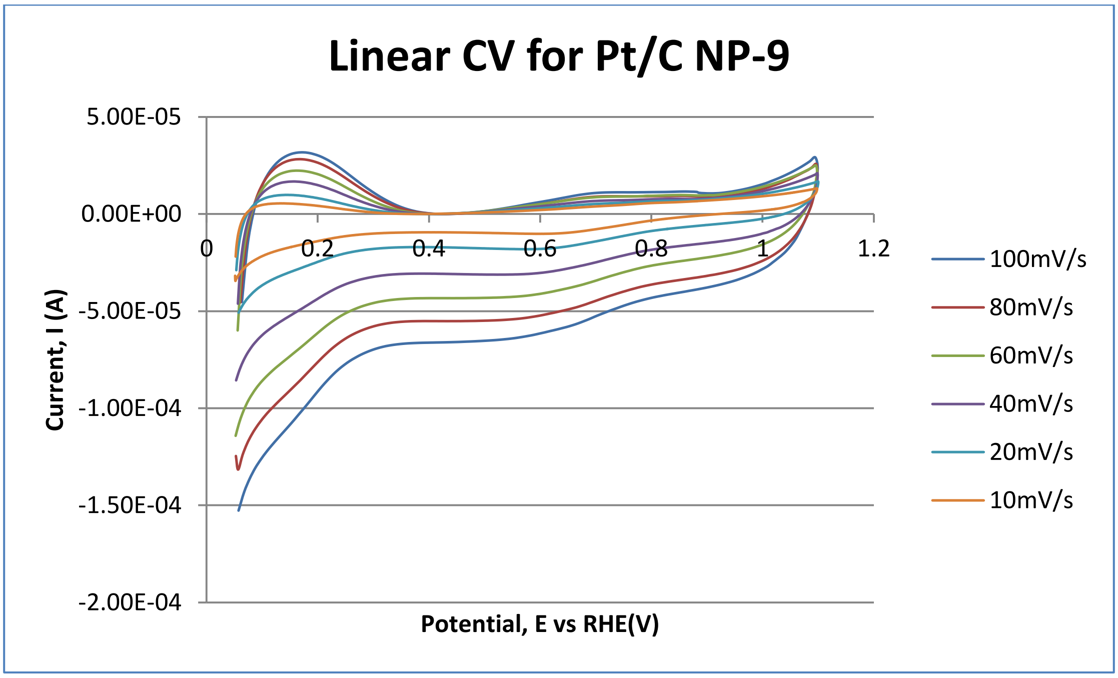

Figure 24 - Linear CV for Pt/C NP-9 in 0.1 M $HClO_4$

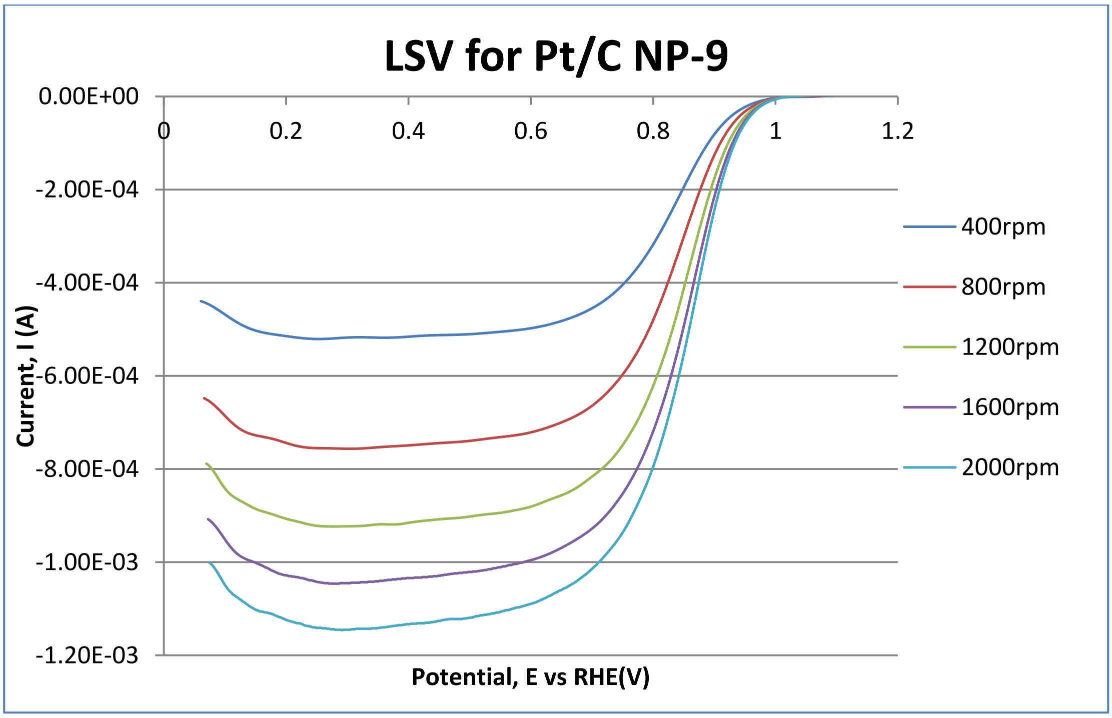

Figure 25 - LSV for Pt/C NP-9 in oxygen saturated 0.1 M $HClO_4$

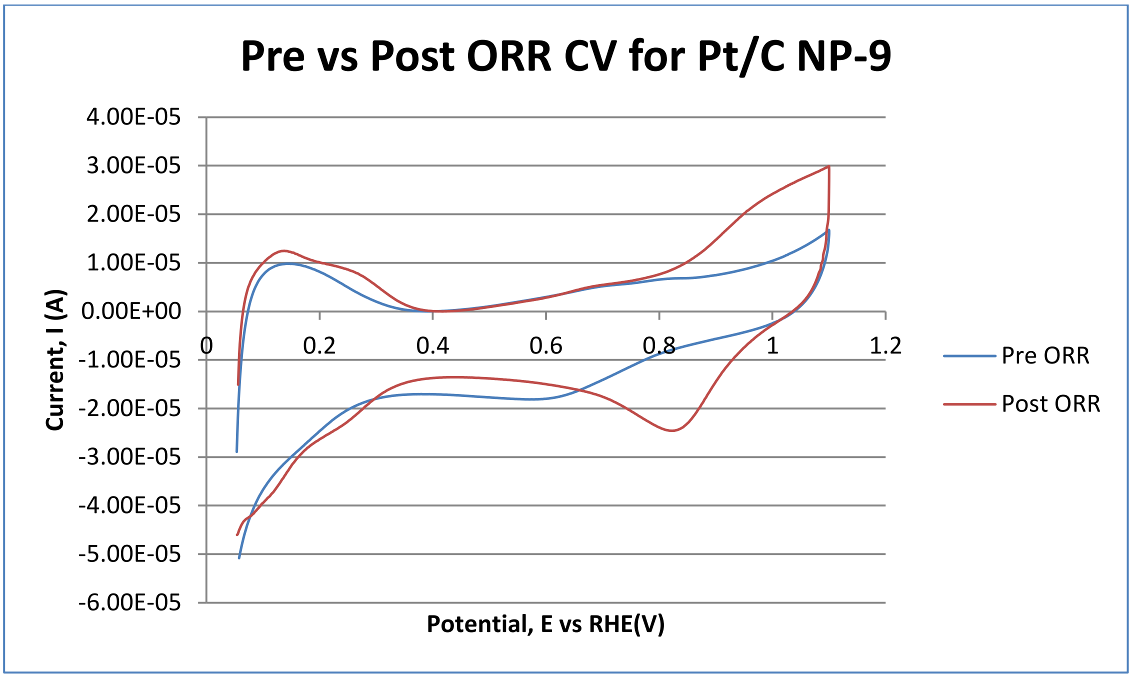

Figure 26 - Pre- vs Post-ORR Linear CV for Pt/C NP-9 in 0.1 M $HClO_4$

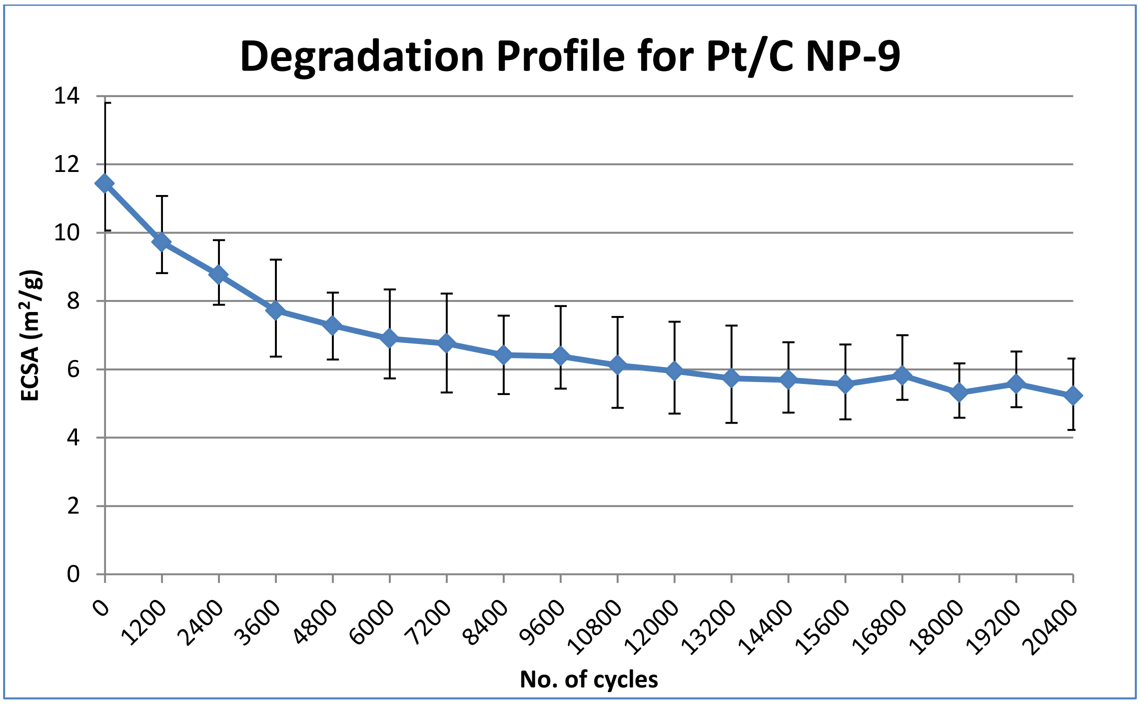

Figure 27 - ADT ECSA profile for Pt/C NP-9 in 0.1 M $HClO_4$

8.2.3 Pt/GO

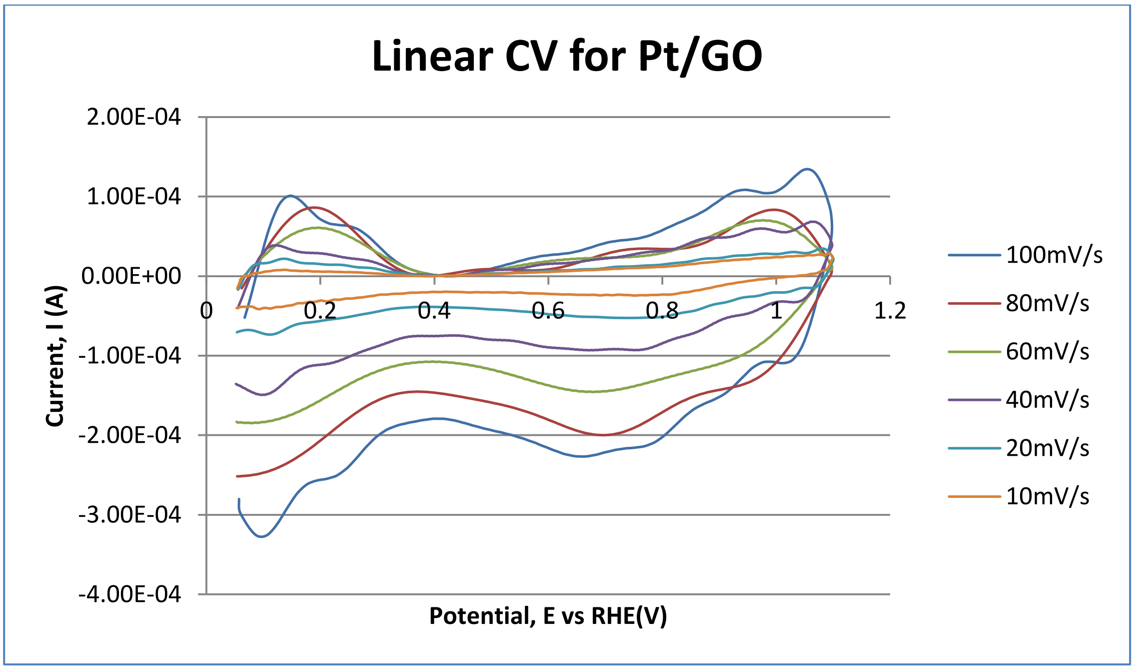

Figure 28 - Linear CV for Pt/GO in 0.1 M $HClO_4$

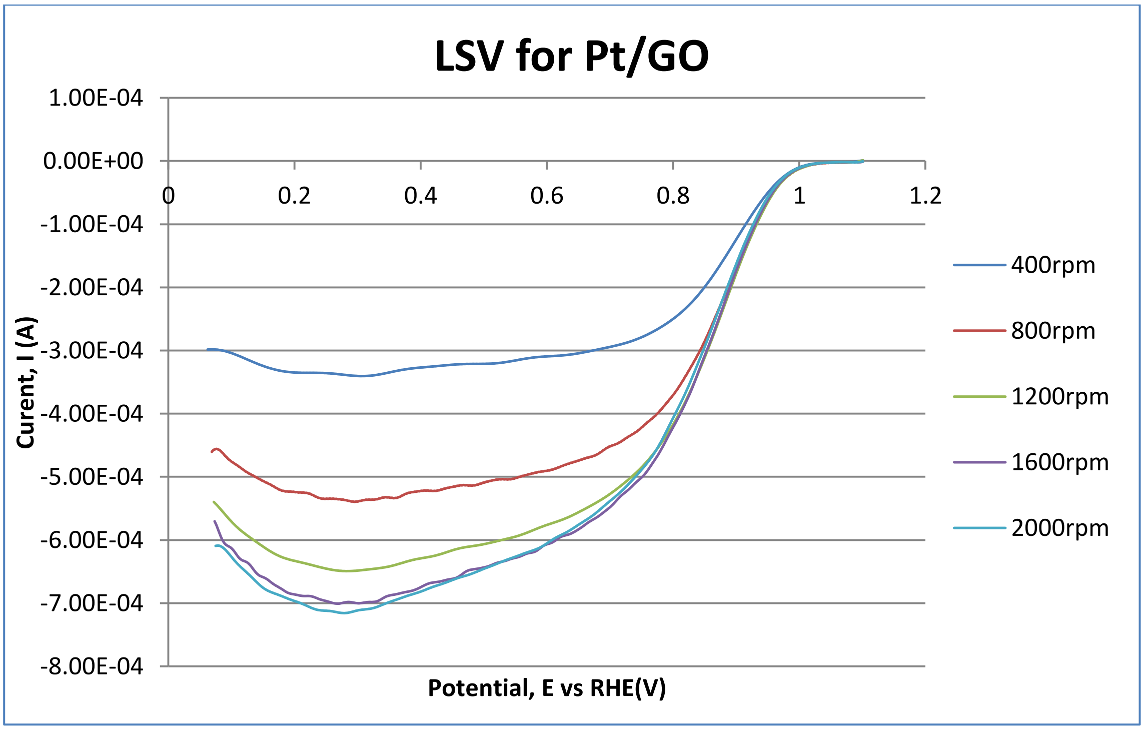

Figure 29 - LSV for Pt/GO in oxygen saturated 0.1 M $HClO_4$

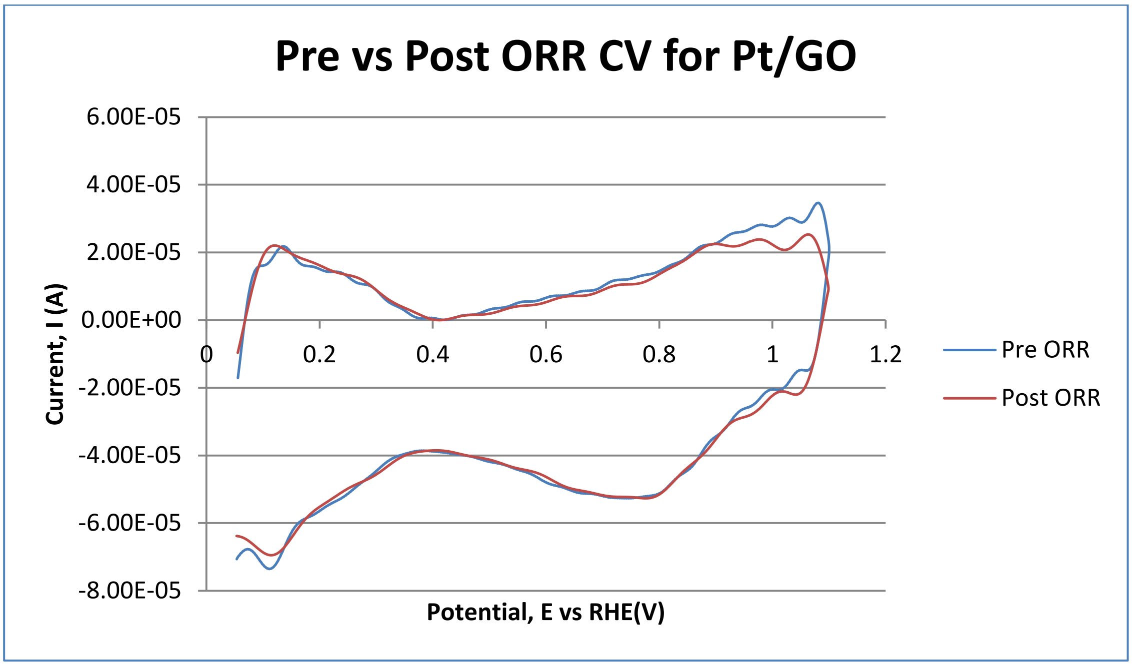

Figure 30 - Pre- vs Post-ORR Linear CV for Pt/GO in 0.1 M $HClO_4$

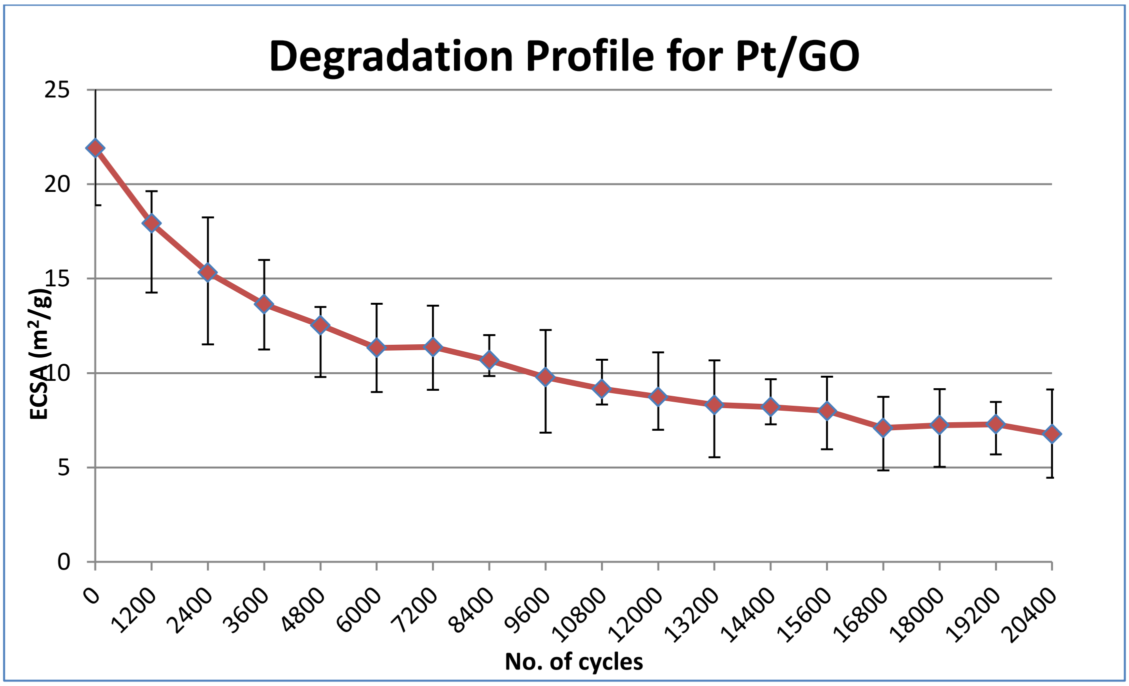

Figure 31 - ADT ECSA profile for Pt/GO in 0.1 M $HClO_4$

8.3 Conferences Attended

This work was presented at

- CATSA 2012 in Langebaan, South Africa, 11-14 November 2012
- ISE 13th Topical Meeting in Pretoria, South Africa, 7-11 April 2013